Lanthanide complexes as redox and ROS/RNS probes: A new paradigm that makes use of redox-reactive and redox non-innocent ligands

D. Mouchel Dit Leguerrier, R. Barré, J.K. K Molloy, F. Thomas, D Mouchel, Dit Leguerrier,] R Barré

Lanthanide complexes as redox and ROS/RNS probes: A new paradigm that makes use of redox-reactive and redox non-innocent ligands

D. Mouchel Dit Leguerrier,[a] R. Barré, [a] J. K. Molloy, [a]* F. Thomas[a]*

Equipe de Chimie Inorganique & Redox

Univ. Grenoble Alpes, CNRS, DCM,

38000 Grenoble, France

Jennifer.molloy@univ-grenoble-alpes.fr, fabrice.thomas@univ-grenoble-alpes.fr

Keywords : Lanthanides, Redox, Probes, Contrast agents, Luminescence, Non-innocent ligands, Redox-reactive ligands

Abstract

Lanthanides complexes are indispensable in fields related to medicine and biology. Their success lies in the great number of unpaired electrons ($4f^7$ configuration of the Gd^{3+} ion) that makes them ideal contrasts agents for magnetic resonance imaging. On the other hand their narrow emission bands and long lifetime of their excited state provide them unique luminescence properties. The aqueous solution chemistry of the lanthanides is dominated by the (+III) oxidation state under oxygenated atmosphere. This severely limits their use as redox probes, and not surprisingly very few redox-switches employing lanthanide ions were reported until 2010. A very promising approach based on redox-reactive and redox non-innocent ligands has recently emerged in the literature, which overcomes this limitation and expands the application of lanthanides to redox monitoring. Herein the ligand acts as a redox-sensor by either changing its oxidation state or reacting with reactive oxygen (or nitrogen) species (ROS/RNS). Its response induces changes in the environment of the lanthanide ion, which acts as a reporter of the redox status. The detection is based on a modification of the magnetic or optical properties of the complexes, with detection by conventional spectroscopic techniques. We summarize in this review article the recent advances in this burgeoning field, with special emphasis on the detection of biological relevant ROS, RNS and redox status.

1. Introduction

The lanthanides or lanthanoids are a series of elements residing in the 'f block' at the bottom of the periodic table. The f block where the lanthanides reside is so called because the f electrons are extremely important for their chemistry. Commonly called "rare earths", they are in fact more abundant than gold. These elements incited modest interest until the 80s, which marked a renewed interest and fast growth of the field. In particular, the distinct properties of the 4f electrons (see below) confer to these elements unique optical and magnetic properties that are currently exploited for many commercial applications. The various fields where lanthanides are unmissable encompass lasers [1], magnets [2], batteries [3], catalysis [4], phosphors [5], security ink [6], medical imaging [7]… This success means that the lanthanides are now considered as strategic choices for a range of applications.

The solution chemistry of the lanthanides is largely dominated by the (+III) oxidation state under oxygenated atmosphere, which has undoubtedly contributed to the original limited interest in these elements [8]. A few noticeable exceptions are those possessing empty, half-filled or filled 4f orbitals. A prototypical example is Eu(II), where the half-filled $4f^7$ shell contributes to the substantial stability of the (+II) oxidation state (in reducing conditions). It must be stressed that most of the other lanthanides have now been characterized in their divalent form due to recent progress in organometallic chemistry, but these forms usually require specific ligands and prevail only under controlled atmosphere [9]. The other classic example of a lanthanide which is stable under an oxidation state different than (+III) is tetravalent cerium. It indeed adopts the stabilizing electronic configuration of xenon, making Ce(IV) a classical oxidant in organic chemistry (cerium ammonium nitrate). The (+IV) oxidation state is now no longer restricted to cerium: Isolable molecular Tb^{4+} complexes were described in 2019, based on a significant lowering of the Ln^{4+}/Ln^{3+} redox potential by coordination to imidophosphorane and siloxide-based ligands [10, 11]. Similarly, Pr^{4+}, Nd^{4+} and Dy^{4+} species were reported [12]. The quest for moieties capable of stabilizing unusual Ln oxidation states is challenging and still actively pursued, but the low denticity of the currently developed ligand platforms induces some limitations (low binding constants due to low chelate effect). Hence designing a lanthanide complex whereby the metal ion is capable of reversibly switching between two oxidation states under physiological conditions yet remains highly challenging.

An elegant approach to provide a lanthanide complex with redox activity consists in associating a redox-reactive or redox non-innocent ligand with the Ln(III) ion. This recent alternative offers exquisite advantages for designing Ln-based redox switches: The high versatility of the redox non-innocent groups allows, for example, a fine control of the targeted redox potentials. Furthermore, the redox-reactive units can be embedded into polydentate and/or macrocyclic platforms, enhancing the binding constants and offering the possibility for additional functionalization. Finally, any lanthanide can be incorporated, which allows the monitoring of redox changes by distinct techniques, or even by targeting different wavelengths when dealing with luminescent metal ions.

The design of redox switches based on lanthanide complexes employing redox-reactive ligands has undergone a fast expansion during the past decade [13-16]. Unprecedented biological applications can now be envisaged, the most promising one being the real-time monitoring of the redox status or related reactive oxygen species (ROS) in cells or tissues by non-invasive methods [13, 17-19] [20]. This interest stems from the fact that an overproduction of ROS or chronic exposure to ROS originating from exogenous sources (xenobiotics, tobacco, alcohol, radiations, extensive pollution…) leads to a disturbance of the redox homeostasis known as oxidative stress [21]. The oxidative stress is believed to favour number of pathologies [22], including cancerization [23], neurodegenerative diseases [24], age related macular degeneration (AMD), cardiovascular diseases, complications of diabetes… Furthermore, conditions of oxidative stress are encountered during inflammatory processes and may be also markers of infections. Hence the development of lanthanide complexes allowing for the real-time monitoring of the redox status by using clinically available techniques would vastly affect the early diagnostic and treatment potential of the above diseases. The aim of this review is to provide the reader with a vast overview of this burgeoning field. We will highlight in the following section the importance of the ROS, oxidative stress and cellular redox homeostasis and next introduce lanthanide ions together with their specific properties that make them ideal candidates for biological imaging. Note that excellent reviews are available in the literature for an in-depth understanding of the lanthanide coordination chemistry and their peculiar spectroscopy [25-27]. Having presented these two important aspects we will provide an exhaustive bibliography of lanthanide complexes based on redox-active ligands that can be used for the detection of ROS/RNS and to monitor redox events. We also include in this review probes that react with thiols, which are proven to reflect the intra or extracellular redox status.

2. ROS, RNS and cellular redox homeostasis

2.1 The different ROS and RNS

The term reactive oxygen species (ROS) refers to compounds resulting from the incomplete reduction or activation of dioxygen [28], as well as reactive products resulting from its attack onto biomolecules (Fig. 1). The ROS family primarily encompasses the superoxide radicals ($O_2^{\bullet-}$), hydroxyl radical ($OH^{\bullet}$) and hydrogen peroxide (H_2O_2). It is completed by singlet oxygen ($^1O_2$), which is photogenerated, and represents a reactive form of dioxygen. Hypochlorous acid (HOCl) is also referred to as ROS, while connections are found between ROS and reactive nitrogen species (RNS) through nitrogen monoxide (NO) and peroxynitrite (ONO_2^-). The products of lipid peroxidation "peroxyl radicals" $LOO^{\bullet}$ are also considered as ROS. ROS (and related RNS) have in common a significant oxidizing ability, and the potential for injuring biological molecules. They exhibit distinct reactivity within a cellular medium [29]: The $OH^{\bullet}$ radical is the most reactive ROS, with a half-life of less than 1 μsec. The reaction volume is about 1 nm, implying that it reacts at the place where it is generated. The $O_2^{\bullet-}$ radicals showed a slightly longer half-life ($t_{1/2}$ = 1-4 μsec), while H_2O_2 is the most stable ROS ($t_{1/2}$ = 1 msec) and can diffuse throughout the medium [30]. NO is a weak and relatively stable oxidant, with half of about 1-10 sec in biological media. Peroxynitrite is a reactive peroxide ($t_{1/2}$ = 10-20 msec)[31] resulting from the fast reaction between NO and superoxide, hence connecting ROS with RNS. Note that the half-lives are given in a cellular medium and can be much longer outside the cells [32].

Strikingly, ROS are paradoxal species, whereby they are highly toxic for cells at high concentration, but conversely act as important signaling molecules at lower "physiological" concentrations [33]. This signaling role implies that they are naturally generated in the cells in a controlled fashion under "normal" conditions.

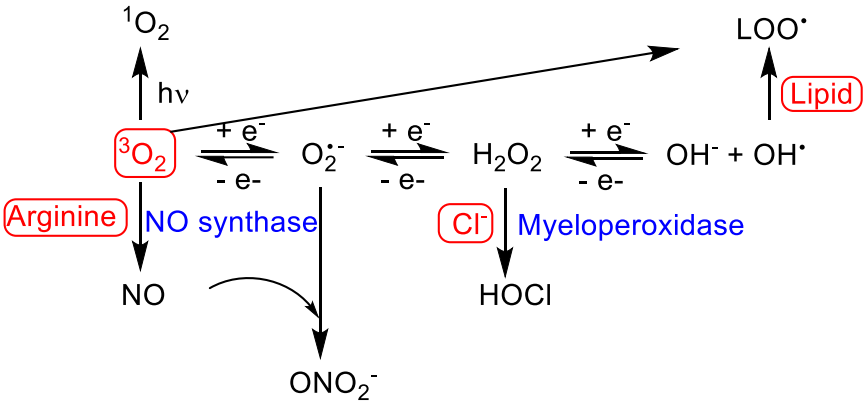

Figure 1. Principal ROS and RNS

2.2 Sources of ROS and RNS

ROS and RNS are generated in distinct organelles of the cells by enzymatic systems (Fig. 2). We will briefly introduce in this section the enzymatic systems mobilized for this purpose.

The major source of cellular ROS is the mitochondria [34]. The mitochondrial respiratory chain normally reduces dioxygen into water by taking up four electrons from two NADH molecules. However, it is estimated that 1-2% of dioxygen is incompletely reduced by the membrane complexes I and III, resulting in the generation of the superoxide anion. The $O_2^{\bullet-}$ radical is readily converted into the less reactive H_2O_2 by the mitochondrial superoxide dismutase. Other important biological sources of ROS are peroxisomes and endoplasmic reticulum [35] through oxidases dedicated to β-oxidation of fatty acids (which mainly release H_2O_2) [36] and cytochrome P450, respectively. Xanthine oxidase [37] catalyzes the last two steps of purine catabolism by converting hypoxanthine to xanthine and xanthine to uric acid in two reactions coupled to the production of H_2O_2 and eventually $O_2^{\bullet-}$ [38].

In humans a significant enzymatic production of ROS is also observed in polymorphonuclear cells during infections. NAD(P)H oxidase, whose main role is dioxygen reduction into $O_2^{\bullet-}$ is activated during the “oxidative burst”. Further coupling of $O_2^{\bullet-}$ release with SOD activity leads to the production of large amounts of H_2O_2, which could be further converted into hypochlorous acid by myeloperoxidase.

Finally, it must be emphasized that the concentration of free copper and iron proved to influence the distribution of ROS. This is due to the occurrence of the Fenton and Haber-Weiss reactions.

For completing this overview, the source of RNS is nitric oxide synthase, which converts L-arginine into citrulline and nitric oxide. The peroxynitrite results from the fast reaction of nitric oxide with $O_2^{\bullet -}$.

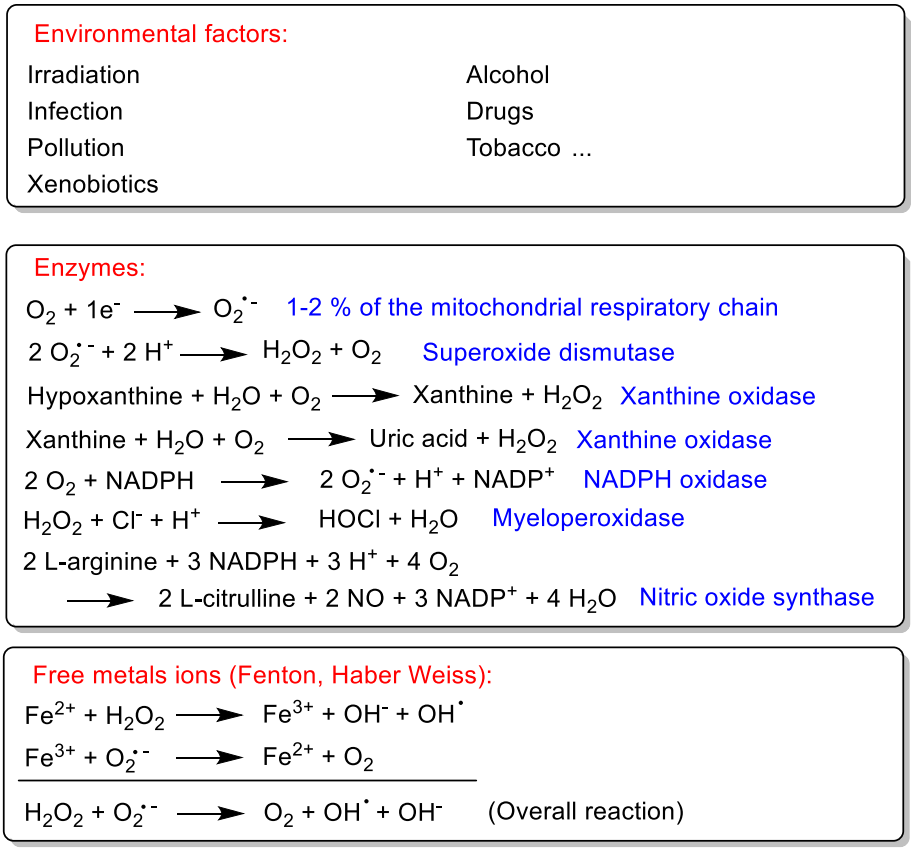

Figure 2. Principal sources of ROS and RNS

2.3 Cellular damage

The cellular targets of ROS are almost all biomolecules: lipids, proteins, sugars, and nucleic acids (Fig. 3). They are damaged by oxidation or nitration and the most important targets are lipids. Increased levels of ROS indeed promote lipid peroxidation, which occurs in a chain reaction [39]. The final products of peroxidation depend on poly-unsaturated fatty acids: They are substantially toxic aldehydes (malondialdehyde and 4-hydroxynonenal, Fig. 3a), as well as F2-isoprostanes which are all recognized markers of oxidative damage. More simple compounds like ethane or ethylene can form, which are both eliminated by the lungs. The biochemical consequences of the oxidation depend

on the nature of the lipids: For membrane lipids the fluidity of the membrane is altered, affecting signal transduction. For circulating lipids the formation of oxidized low-density lipoprotein (LDL, often refers to “bad” cholesterol) is observed, which can accumulate under the form of atheromatous plaques causing atherosclerosis.

The proteins can also undergo oxidation [40]: The targets are both amino acid residues (Fig. 3b) and cofactors. Further chemical consequences are cross-linking, misfolding and cleavages. In general, the oxidation makes the proteins more hydrophobic, and hence more prone to aggregation. Notably, the oxidized proteins are more sensitive to proteolysis than unmodified ones, and consequently more easily eliminated by the proteasomes.

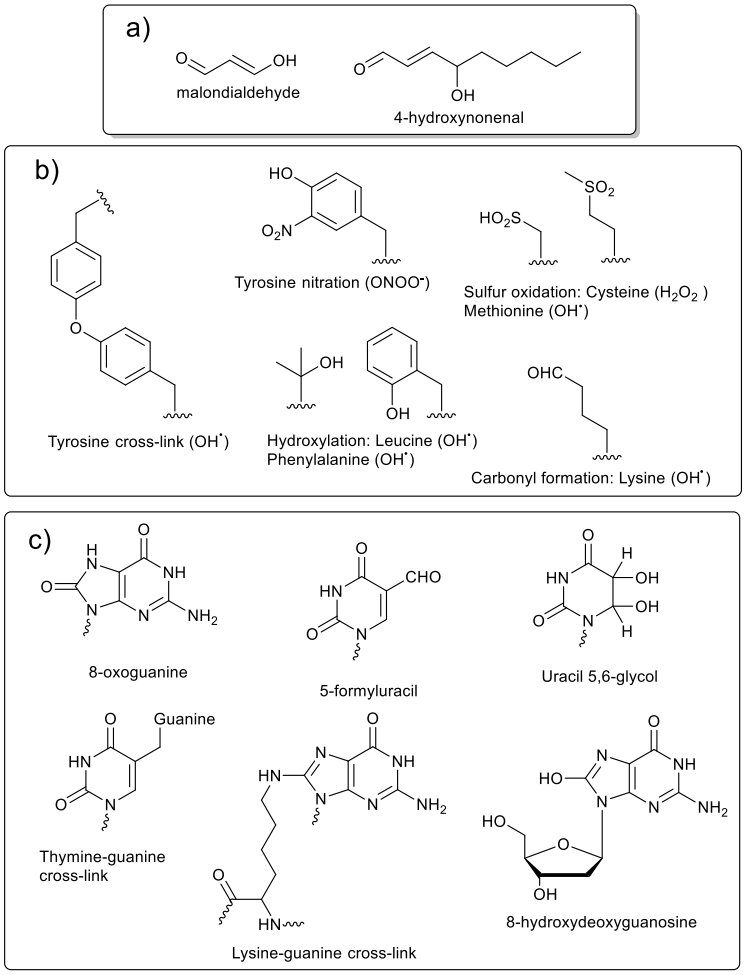

Figure 3. Selected examples of oxidative damages to biomolecules. a) Lipids; b) amino acids (with ROS involved in the reaction); c) nucleic acids

Nucleic acids are the other important targets of ROS [41] .The most common attack is achieved by $OH^{\bullet}$, while $^1O_2$ reacts with guanine only. H_2O_2 and $O_2^{\bullet -}$ do not react with bases at all. Over 100 oxidatively generated lesions were identified in DNA, which include: bases, leading to modified bases (Fig. 3c); oxidized sugars, leading to strand cleavage; attack of the bond between the deoxyribose and the base, affording abasic sites; formation of adducts with either oxidized lipids or neighbouring proteins such as histones and polymerases (through the guanidine function of lysines). Amongst the lesions identified the most common ones are 8-hydroxydeoxyguanosine and 8-oxoguanine, the first being a recognized marker of oxidative stress (Fig. 3c). DNA is not the only nucleic acid target of ROS. RNAs are in fact more often oxidized than DNA due to their cellular distribution, closer to ROS producing sites. The most common damage is 8-hydroxyguanosine, the pendent of 8-hydroxydeoxyguanosine in the RNA series. A consequence of severe attack by ROS is ribosomal dysfunction and hence an altered protein production.

Reactive nitrogen species (RNS) react through peroxynitrite mostly with proteins. Thiols and tyrosines are the main targets, with 3-nitrotyrosine being a characteristic oxidative modification.[42]

2.4 Antioxidant systems

In order to neutralize excess ROS and hence prevent injury to biomolecules the cells have developed an integrated system (Fig. 4) based on enzymes and antioxidant molecules. The interplay between these actors is essential for scavenging ROS of distinct half-life and localization.

The enzyme superoxide dismutase catalyzes the fast disproportionation of superoxide into H_2O_2 and O_2 [43, 44], while catalases catalyze disproportionation of H_2O_2 into H_2O and O_2 [45] and peroxidases exploit the oxidizing power of H_2O_2 to oxidize substrates or enzymes [46]. Thioredoxins operate slightly differently as they usually catalyze the cysteine thiol-disulfide exchange [47]. Therefore, they are capable of reducing disulfide bonds generated in proteins by hydrogen peroxide.

The most abundant cytosolic antioxidant is glutathione (GSH), which can account for more than 90% of the total nonprotein sulfur in a cell [48]. Its sulfhydryl group is redox-active and capable of shuttling between the reduced (-SH) and oxidized (-S-S-) states, both being stable (*in vivo* potentials of -260 mV to -150 mV). In normal conditions the

major form of glutathione is the reduced one, GSH (90-99 %), which can either directly neutralize $OH^{\bullet}$ or act as cofactor in the enzymatic neutralization (glutathione peroxidase) of lipid peroxides and H_2O_2. Acid ascorbic is believed to be the main antioxidant in the plasma.[49] It directly quenches a great variety of ROS/RNS, including the reactive $OH^{\bullet}$ and $O_2^{\bullet -}$ radicals, but not the lipid peroxy radical $LOO^{\bullet}$. In contrast to vitamin C, vitamin E (α-tocopherol) is lipophilic and can localize in the membranes [50]. It plays a crucial role in preventing the propagation of lipid peroxidation through scavenging of the peroxy radical $LOO^{\bullet}$.

Other recognized antioxidants are phenolic compounds (flavonoids), with multiple actions (including scavenging of radicals, metal chelation…), carotenoids which scavenge $^1O_2$ and quench the excited chlorophyll molecule in plants to prevent the formation of $^1O_2$ and uric acid. Uric acid is present in relatively large amount in plasma (200–400 μM), where it acts as an efficient scavenger of $^1O_2$, $LOO^{\bullet}$ and $OH^{\bullet}$ [51]. Its hydrophilic nature means that it reacts only with hydrophilic $LOO^{\bullet}$ radicals and hence is not capable of stopping the peroxidation of lipids as does vitamin E.

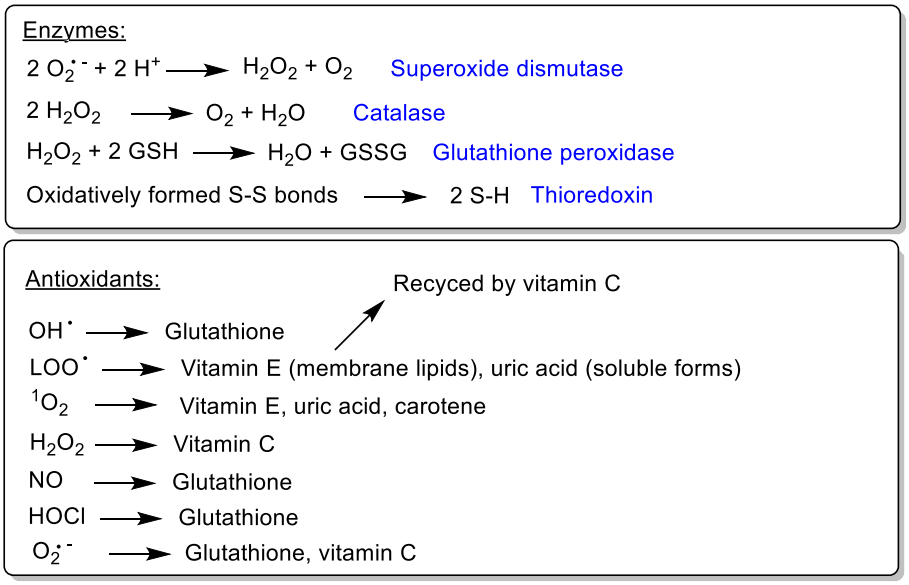

Figure 4. Integrated system for ROS neutralization

2.5 Redox homeostasis and diseases

The cellular redox homeostasis is tightly regulated (buffered) owing to a subtle balance between ROS/RNS and antioxidant defense. Under normal conditions the production of ROS/RNS is

adaptive and controlled. When ROS/RNS are produced in excess the cellular antioxidant systems can be overwhelmed. The redox homeostasis is then disrupted, leading to an oxidative stress. Such situations are favored by some environmental stimuli like the presence of some drugs (gentamycin, and bleomycin…), pollution, tobacco, alcohol, inflammation and radiations. An important consequence of oxidative stress is ageing [22, 52]: Progressive accumulation of oxidative damage to biomolecules due to a chronic oxidative stress, ultimately results in a loss of organ function. Oxidative stress is also believed to be involved in more than 50 diseases: The chronic hyperglycemia observed in diabetic patients induces oxidative tissue-damaging effects, which may be responsible for complications of the diabetes [53]. Cardiovascular diseases proved to be correlated to atherosclerosis and the level of oxidized LDL [54], [55] [22]. The Alzheimers disease is favoured by an abnormal mitochondrial ROS production, combined with altered homeostasis of some metals [56]. Carcinogenesis occurs according to a multistep process, where ROS play important roles [23]. As an example oxidative damage to macromolecules, especially DNA mutations widely contribute to tumor initiation [57] when they are preceded by cell division (fixation of the mutation). Further mutations and signalling events contribute to the subsequent steps of tumorization [58]. Oxidative stress is also contributing to the development of age related macular degeneration (AMD) [59], as verified by the high levels of malondialdehyde, protein carbonyls, and 8-hydroxy-2-deoxyguanosine (oxidative stress markers) found in the blood serum from AMD patients [60]. Perhaps the most surprising, connections were also established between oxidative stress and infertility [61]. Of course, RNS are connected to ROS, and their over-production [62] is held responsible for similar diseases including cancers [63], Parkinson's, and Alzheimer's disease [64, 65].

3. Principal methods of imaging using lanthanide complexes

3.1 Main scope of imaging

In order to study in detail, the redox balance within cells, tissues and in a whole organism it is essential to find an appropriate technique. We will focus in the next sections on lanthanide complexes and their dedicated spectroscopic techniques, which recently proved to be powerful tools when the ligand was adequately engineered.

There are few techniques showing potential for detection of biochemical species *in vivo*. Medical imaging is used to generate images of the human body, which provides essential information on position and morphology for diagnosis and therapy [66, 67]. Molecular imaging has recently become the principal method of detection when speaking about small species often responsible for major pathological illnesses [68]. It is gaining intense interest due to the potential to image and investigate the disruption of biochemical processes and their potential development into dangerous diseases [68, 69]. Unlike classical imaging techniques it can characterise tissues and their physico- chemical properties (pH, concentrations of cations, metals, metabolites) [70]. Some characteristic species are present long before the physical manifestations of the diseases are visible. Consequently, molecular imaging is key to make diagnostic breakthroughs for disease detection and therapy. Two main techniques in molecular imaging have been vastly studied, magnetic resonance imaging and luminescence imaging, the detection of active species evoking a luminescent response or a magnetic response. Each method presents particular advantages but also limitations which will be discussed below.

3.2 Magnetic Resonance Imaging (MRI)

Typical magnetic resonance imaging uses the density and relaxation of water protons to induce contrast in different chemical environments and thus generate a contrast image [71]. Paramagnetic complexes which are used as contrast agents will reduce the longitudinal T1 and transverse T2 relaxation times in the tissues leading to increased contrast [72]. These contrast agents improve resolution for the imaging of position and morphology in the human body. The injection of such commercial contrast agents allows random distribution, meaning their aid in the visualisation of pathology is mainly morphological or physiological.

These contrasts agents depend on the strongly paramagnetic nature of the lanthanide ion, mostly Gd^{III} [73]. The fast relaxation time of the Gd^{III} metal ion has a large effect on the water proton relaxation, reducing the longitudinal T1 and transverse T2 relaxation times, thus increasing contrast, generating an image in magnetic resonance imaging [74]. The contrast potential of a contrast agent or its efficiency can be denoted by r_1 or the relaxivity, which is the relaxation enhancement of the water proton relaxation rate in the presence of 1mM of contrast agent [75]. There are two major contributions to the relaxivity of a contrast agent, the inner sphere contribution and outer sphere contribution.

The inner sphere mechanism is sensitive to ligand design and thus can be distinctly altered via successful design of the complexes of Gd^{III}. The inner sphere relaxivity is directly proportional to the coordinated water molecules q, and depends on the rate of exchange of water molecules on the metal centre and the bulk k_{ex} and the rotational dynamics of the complexes, the rotational correlation time τ_R. These parameters can be controlled via specific design of the ligand around the metal ion, this allows the alteration of the efficacy of the contrast agent as a function of ligand design.

Recently, intense research has been focused on the development of molecular contrast imaging agents or agents that are capable of detection of changes in local environments in tissues. Such agents have been reported for monitoring pH and temperature change, detection of different species, and maybe more counter-intuitive owing to the redox-innocent of the gadolinium ion, redox status [16, 76-78].

3.3 Chemical Exchange Saturation Transfer (CEST) and PARACEST

Chemical Exchange Saturation Transfer represents a very interesting alternative to classic relaxivity based contrast mechanisms in responsive probes [79, 80]. 'CEST' probes possess one or more exchangeable protons in slow to intermediate exchange with the bulk water protons, such as the –NH of amides, - OH of alcohols ($k_{ex} \leq \Delta\omega$, where $\Delta\omega$ is the chemical shift difference between the two proton pools) [81]. In this technique the slowly exchanging protons of the contrast agent are saturated by selective radiofrequency pulses, which quench the exchangeable proton signal, and also affect the bulk H_2O signal due to exchange [82]. This water proton difference in intensity can be imaged in an MR experiment. The main advantage with respect to classic Gd^{III} based probes is that the contrast is selectively turned on upon specific irradiation. It uses paramagnetic metal ions that can induce paramagnetic shifts of the protons but not have a particularly strong relaxation effect such as that of Gd^{III}. This irradiation, followed by exchange, mean these probes have a fundamental difference with respect to classic MRI mechanisms; they can possess several moieties with each a selected irradiation frequency thus permitting several 'signals' in the same probe [83].

PARACEST CAs use the paramagnetic properties of lanthanide ions to strongly shift the exchangeable protons frequency and induce a selectivity [84]. The parameters involved in a CEST experiment are the proton exchange rate $k_{ex,}$ the power of the pre saturation pulse applied in the experiment, B2, and the proton relaxation times in the two

exchanging pools of protons [85]. Provided complete saturation occurs the net magnetisation of the bulk water protons can be shown as

$$\frac{M_Z}{M_0} = \left(1 + \frac{C\ n\ T_1}{111\ \tau_M}\right)^{-1}$$

where τ_M is the proton resident lifetime, C is the probe concentration, n is the number of equivalent exchanging protons per molecule and T_1 is the spin lattice relaxation time. The optimal exchange rate providing a maximum CEST signal is related to B2 according to $k_{ex} = 2\ \pi B_2$ [80].

The development of CEST active probes with redox activity can allow a redox process that occurs on the metal centre of the ligand. The change in magnetic properties of the metal can lead to resonance frequency modification and of the relaxation rate of the ligand protons. It can potentially lead to chemical shift changes.

3.4 Luminescence

The second and maybe more prevalent means of responsive detection is via luminescence. Responsive probes can affect the emissive excited state of the probes inducing changes in the intensity, in spectral shape or in the luminescent lifetimes [86, 87]. Luminescence spectroscopy is an extremely interesting detection method due to the potential of the luminescence to give selective, specific signals on a short timescale, which allows remarkably low detection limits, particularly useful to diagnose and analyse cellular systems [88, 89]. Imaging using luminescence spectroscopy has attracted increasing interest compared to MRI imaging due to its higher sensitivity and specificity [17]. The vast library of potential emissive probes currently under development based on organic fluorophores, nanoparticles, transition metal complexes or lanthanide-based probes can lend this technique to the visualisation of physiological processes in the human body [89, 90].

Imaging using luminescence can utilise the intensity of emission, the spectral signature and the lifetimes. A luminescent response depends on several aspects of the excited state of the luminophore (singlet and triplet excited levels), the lifetime of each excited state, the deactivation/activation processes involved to allow a response as a function of conditions or the proximity of analytes [86]. In order to form a responsive probe one of the excited states must be susceptible to stimulus, giving one of the methods of response discussed above. The emission spectra are very sensitive to environment and can give

very efficient responses in detection. Luminescent lifetimes can also be an invaluable method to extract information, due to the sensitivity of the lifetimes but also its independence of concentration. A luminescent lifetime is the average time that an excited chromophore remains in its excited state. Its advantage relies on the principle that different chromophores with similar emission wavelengths can be distinguished by their respective lifetime decays.

Classic organic fluorophores suffer from very short lifetimes due to population of largely single excited states with fast decay pathways. This characteristic can limit very significantly the measurement potential. The development of fluorescent probes for detection has been extensively discussed based on simple fluorescent organic compounds [90]. However, there are several drawbacks with this method, in general while fluorescent probes are extremely sensitive they are usually very short lived and are predominantly short wavelength emitters, which is obviously a great concern for use in competitive biological media. This signifies there is limited penetration in tissues, so this technique is much more suited to cellular imaging and *in vitro* testing, although attempts to find NIR probes which can rely on higher wavelength excitation or on two photons excitation are in progress [91, 92]. The development of probes capable of longer lived and more substantial emission is a subject of intense development,[93] to be discussed further in the following sections.

4. Lanthanide ions for imaging

4.1 Specific properties of lanthanide ions for achieving selective detection

Lanthanide chemistry is dominated predominantly by the (+III) oxidation state although other less prevalent oxidation states are possible (see above). These Ln^{III} ions have electronic configurations which depend on $[Xe]4f^{n}$. They present long relaxation times and very long lifetimes, meaning that the fluorescence of the background medium will be quenched before the luminescence of the lanthanide ion, Fig 5 [94]. The lanthanide ions also possess the distinctive line like emission bands, which makes their specific detection easier [95].

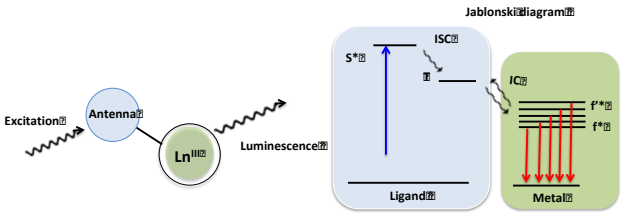

Figure 5. Jablonski diagram showing population of Ln^{III} excited state via energy transfer

These ions suffer from parity forbidden f-f transitions (Laporte forbidden) resulting in extremely weak extinction coefficients typically on the order of 100 $M^{-1}cm^{-1}$. This drawback means direct excitation of the lanthanides is difficult making them difficult to excite and very weakly luminescent. In order to increase the sensitisation of the lanthanide excited state for luminescence we then need to rely on their chelation to appropriate ligands whereby an organic chromophore can take part in sensitised emission or the antenna effect, Fig 6 [96]. The process involves excitation of the chromophore with incident light to populate the singlet excited state. This state can then result in population of the lanthanide excited state or formation of a triplet state whereby intramolecular energy transfer then occurs from the triplet, see Jablonski in Fig. 5, to populates the Ln^{III} state with subsequent luminescence. This chromophore must possess a high molar absorption coefficient meaning excitation can efficiently populate its excited state. The choice of antenna and its photophysical properties are thus very important, especially its molar absorptivity (potential to absorb photons), possibility of charge transfer, the position of both the singlet and triplet energy levels and the size of this energy gap which determines the possibility for intersystem crossing. These factors will all determine the efficacy of excited state population. The energy level of the antenna is important as small S_1 to T_1 energy gaps promote faster intersystem crossing processes which favour them over the radiative deactivation of the S_1 level.

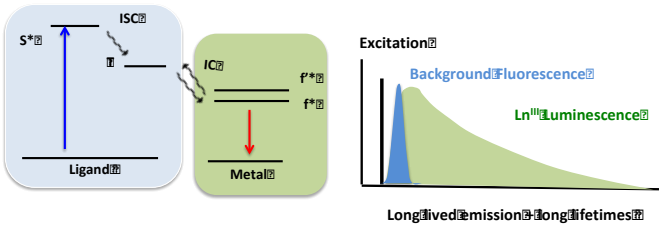

Figure 6. a) Population of lanthanide excited state b) Delayed luminescence and long emission lifetime

The design of the lanthanide complexes is thus extremely important [90, 97]. The triplet level of the antenna needs to be thus ideally situated with respect to the lanthanide excited state in order to achieve successful sensitisation. The donor must lie within $10k_bT$ (approx. 2050 cm^{-1}) higher than that of the excited lanthanide energy level to promote intramolecular energy transfer. All of these considerations determine the choice of excitation wavelength, the efficiency of the triplet formation after inter system crossing and the intramolecular energy transfer to populate the excited state of the lanthanide. The sensitisation of the lanthanide excited state via the antenna proceeds via the Jablonski diagram schematically represented in Fig. 6, followed by relaxation with emission of the lanthanide species [98].

Once sensitised the emission of the lanthanide presents several important distinctive aspects of lanthanide luminescence such as long wavelength emissions spanning the visible and NIR regions depending on the Ln^{III} [99], very sharp line like emissions and long lived excited states. These transitions mean that the luminescence is longer than the autofluorescence of the biological media. This bypass of the biological background improves signal to noise and thus makes them a fascinating alternative to traditional fluorescent probes (Fig. 6) [20].

4.2 Lanthanide complexes as redox responsive agents

In order to report on changes in their redox environment the complexes must either shuttle between two oxidation states in the investigated potential range, each having distinct spectroscopic signature, or directly react with a species responsible or generated by the un-balanced redox status. This reaction can be chemical or not. In this latter case interaction may cause modification of the lifetime of the excited state, alteration of the relaxation rates… The induced phenomenon will obviously be appropriate to the technique used for the detection.

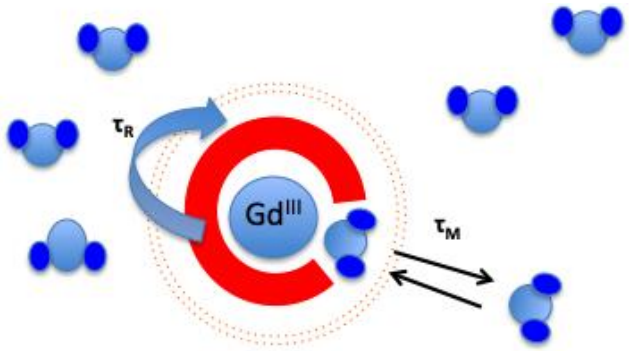

Figure 7. Gd^{III} complex showing water exchange and rotational correlation time

Lanthanide ions exist mainly in their (+III) oxidation state therefore cannot undergo redox changes or reactivity with redox functions [100]. The redox-response is therefore on the ligand, which transmits the information to the lanthanide, this latter acting as a reporter.

As stated previously the relaxivity calculates the effect of the contrast agents on the water relaxation. This relaxivity depends on the number of water molecules, the water exchange rate and the rotational correlation time. Responsive agents can affect any one of these factors. To monitor a redox change by MRI there are potentially two pathways. Reversible changes in conformation upon reaction with ROS, can adjust the access of water molecules to the coordination centre. Alternatively, a change in intermolecular interactions modifies the interactions between complexes thus increasing or decreasing the rotational correlation time. These two effects show dramatic changes in the r_1 as they are the two major factors for modification of the relaxivity of a metal complex [16]. Modifying the ligand structure can thus induce dramatic changes in contrast with addition of water molecules and increased rotational time gaining in intensity (Fig. 7)).

Luminescent-based redox monitoring is particularly interesting as it is very sensitive to external stimuli. Using lanthanides as reporters can lower the detection limit due to the line like emission bands and the sensitivity of the emission to the environment. The modification of the Ln^{III} luminescence can be achieved via modification of three possible excited states in the complex, the singlet and triplet of the ligand and the excited level of the lanthanide. In the lanthanide complexes modification of the ligand structure which acts as the antenna for lanthanide excited state population can result in modification of one or more of these three states, resulting in drastic changes in luminescence behaviour. These possible modifications van be achieved via; i) modification of the geometry around the metal centre ii) altering the population of the

lanthanide by chemical modification of the antenna which can quench or sensitise the luminescence iii) displacement of OH or NH quenchers in the coordination sphere. Thus, ligand design is extremely important to ensure possibility of a chemical or redox reaction to allow such changes to influence the lanthanide behaviour.

5. Detection of molecular oxygen

Molecular dioxygen is the most evident target when we are dealing with the detection of oxidative stress and tissue activity. It is indeed the unique precursor of all the ROS and further contributes to the intra and extracellular redox status. Perturbation of the oxygen levels can be markers of pathologies: solid tumours demonstrate hypoxic regions and are surrounded by aberrant vasculature aimed at supplying them with nutrients and oxygen essential for their fast growing [101] while ischemia, oxygen starvation could cause or result from heart disease.

Dioxygen can adopt two electronic structures: Triplet dioxygen $^3O_2$, which is the ground spin state and hence the common form, and singlet dioxygen $^1O_2$, which is a closed-shell excited state accessible only under certain conditions. Because of their distinct reactivities and properties the methodologies developed for their detection will differ significantly. We will first discuss the detection of the unreactive triplet dioxygen and next focus on the highly reactive singlet dioxygen.

5.1 Triplet dioxygen $^3O_2$

The ground state of dioxygen is $^3O_2$, and because of its diradical nature it is poorly reactive. It is therefore difficult to base its detection on a chemical reaction with the probe. The detection of $^3O_2$ is essentially based on two strategies, optical and magnetic. In given cases dioxygen can quench the triplet state of sensitizing units, which results in modification of the energy transfer path in luminescence phenomena. Optical techniques can thus be used for the detection. Alternatively, the presence of paramagnetic dioxygen in the vicinity of paramagnetic complexes can alter significantly the complex relaxation rates and hence induce a response in MRI.

5.1.1 Luminescence-based detection of $^3O_2$

In classical sensitizing cases, population of the Ln^{III} occurs via energy transfer from a ligand triplet state to the lanthanide excited state, both rapidly and irreversibly. Hence the luminescence properties of the metal are in theory independent of oxygen

concentration level. When there is a close energy match between the triplet ligand state and the lanthanide emissive state, a thermal repopulation is however possible. In this case collisional quenching of the triplet state with oxygen might occur, which led to a drastic quenching of luminescence. This phenomenon was exploited for the turn OFF detection of O_2 with several lanthanide probes. In the early 2009 Parker et al. reported the mononuclear complex **1** (Fig. 8) [102]. The excitation of the azaxanthone chromophore leads to population of its triplet state, which is sensitive to quenching by triplet oxygen. The emission of **1** was found to be sensitive to oxygen, whereas that of the europium analog was not, allowing for ratiometric detection of O_2. This was achieved by using a mixture of **1** and its europium analog in aqueous media, through the ratio of the Eu (603–610 nm) to Tb emissions (515–525 nm). Other monometallic complexes operating in a similar way were reported, and were mostly developed on DOTA platforms [102-110].

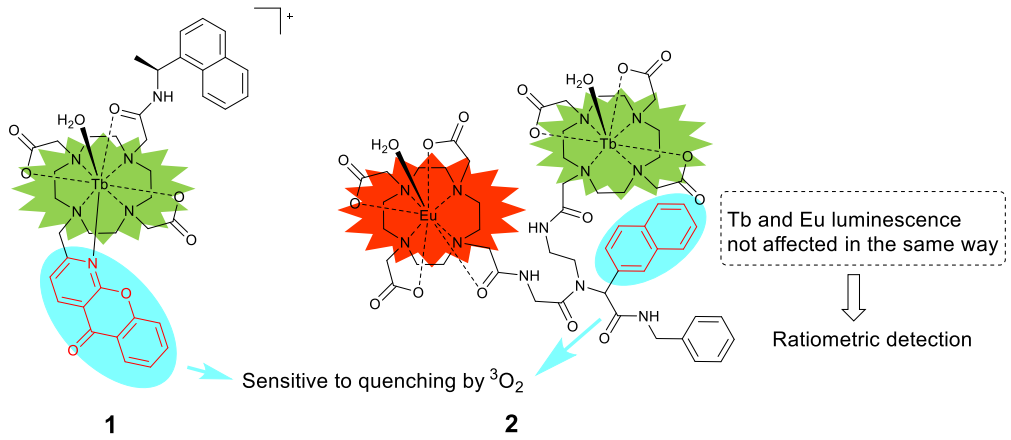

Figure 8. Lanthanide complexes for luminescence detection of triplet oxygen

Later, Faulkner and co-workers reported hetero bimetallic lanthanide complexes such as **2** (Fig. 8) as ratiometric probes for determination of dioxygen concentration. The dinuclear complex **2** associates two DO3A moieties and a naphthyl chromophore [111]. This latter is used to sensitize terbium and europium ions, which are not equidistant. In degassed solution (absence of O_2) **2** shows the classical luminescence emission spectrum of both metal ions. In aerated solution, the Tb^{3+} luminescence is quenched by 50% approximately, while Eu^{3+} luminescence is not affected. Hence both lanthanide ions are not affected in the same manner by oxygen concentration. In addition, the extent of

quenching of the terbium luminescence depends on the oxygen concentration. This allows for a ratiometric measurement of molecular oxygen based on the intensity ratio between the two luminescent responses.

5.1.2 MRI-based detection of $^3O_2$

Real time and *in vivo* detection of molecular oxygen by using MRI was pioneered by Aime and co-workers. Their method is based on the difference of relaxivity between a gadolinium complex loaded on oxy or deoxy haemoglobin [112]. In order to obtain a ratiometric probe, a mixture of two gadolinium complexes is injected. Complex **3** acts as an oxygen responsive probe, whereas **4**-labeled red blood cells (RBC) are used as local probes for determining the RBC concentration (Fig. 9). Complex **3** had a higher affinity (around 5 times) for deoxy-hemoglobin (deoxy-Hb) in comparison to oxy-hemoglobin (Oxy-Hb). The deoxy-Hb/**3** adduct has a relaxivity of 37.5 $mM^{-1}.s^{-1}$ which is seven time higher than free **3**. Upon oxygenation the deoxy-Hb/**3** adduct is converted into oxy-Hb/**3**, which shows a lower relaxivity (around 23 $mM^{-1}.s^{-1}$). This difference of relaxivity between oxy and deoxy-Hb/**3**, combined with a determination of the local concentration of **4** allows for the generation of an MRI-relative de-oxygenation map.

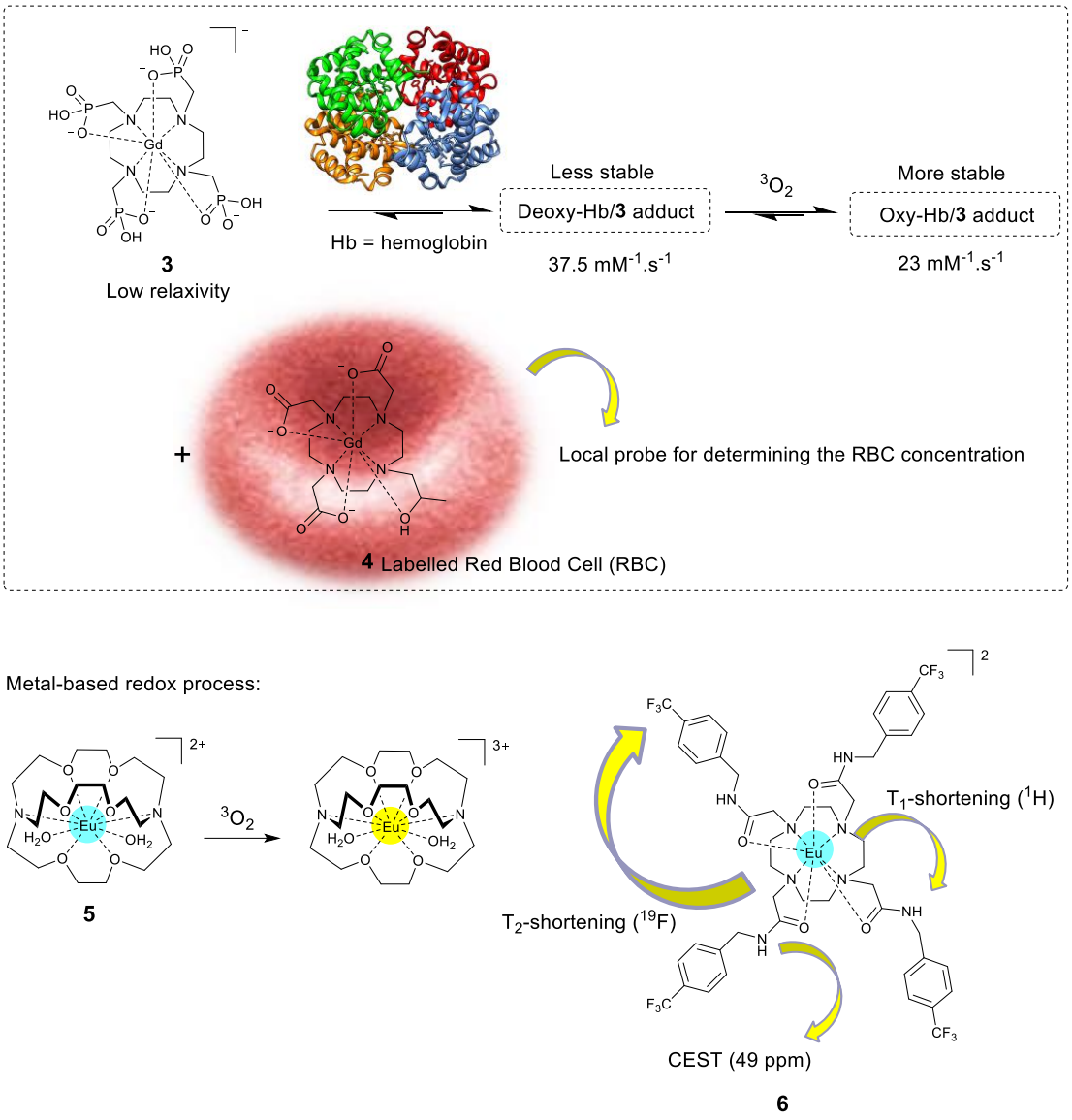

Figure 9. Lanthanide complexes for MRI detection of $^3O_2$

A second method was developed. It is based on the modulation of magnetic properties of the lanthanide ion upon oxidation. Although slightly out of the scope of the present review because this method employs an innocent ligand, it represents a nice comparison between systems involving a metal- and ligand-responsive system. Only europium can undergo redox events as aquo complex (oxidation of Eu^{2+} to Eu^{3+}), hence this method is restricted to this metal. Two types of complexes were designed: europium cryptates (**5** in Fig. 9) [113, 114] and europium DOTA fluorinated tetraamides such as **6** (Fig. 9) [115]. The first group has been proposed as a probe sensitive to pO_2, but the in vivo application has not been undertaken, presumably due to a mismatch between the

Eu^{3+}/Eu^{2+} redox potential and the physiological potential window. Complex **6** was found to be an interesting trimodal probe ($^{1}H/^{19}F$ MRI/CEST). Basically Eu^{2+} is isoelectronic with Gd^{3+} and therefore acts as a T_1-shortening element for proton. This causes a turn ON positive contrast in ^{1}H-MRI. Furthermore, Eu^{2+} also acts as T_2 (transverse relaxation time) shortening element for ^{19}F. As a consequence, it causes line-broadening effects up to the disappearance of the ^{19}F peaks. Air exposure of the complex results in the oxidation of Eu^{2+} into Eu^{3+} that does not affect the ^{1}H and ^{19}F resonances in the same way. As an example no signal can be yet observed in ^{1}H-MRI (turn OFF probe) upon oxidation, while the relaxivity increases from 2.3 to 5.5 $mM^{-1}.s^{-1}$ between 15 and 43°C. Conversely, this complex can act- as a turn ON probe in ^{19}F and CEST imaging. Indeed, a singlet appears at -62.1 ppm in the ^{19}F NMR spectrum upon oxidation, which corresponds to twelve fluorine atoms (using sodium triflate as reference). Similarly to other Eu^{III}-tetraamide complexes, a CEST signal is observed at 49 ppm. Interestingly the trimodal detection was also found to be temperature dependant.

5.2 Singlet oxygen $^{1}O_2$

Singlet oxygen $^{1}O_2$ is the lowest excited electronic state of molecular oxygen. In contrast with $^{3}O_2$ wherein two electrons of similar spin are placed in two degenerate orbitals the two electrons are herein paired in a single of them. It can be generated chemically or after Infra-red irradiation in the presence of a sensitizer. Singlet oxygen is highly reactive and toxic for cellular material (DNA, proteins…) and tissues. It has an important application in photodynamic therapy (PDT), whereby $^{1}O_2$ is generated directly into tumor cells by irradiation, resulting in their destruction. Monitoring singlet oxygen levels by specific, non-invasive and in-vivo methods is therefore an important domain of research [116]. All the reported singlet oxygen detection methods using lanthanide complexes are subsequently based on a selective reactivity between $^{1}O_2$ and a chemical function of the ligand. The anthryl moiety has been widely investigated for this purpose and its modification upon reaction will be a basis for detection by luminescence,[117, 118] and CEST techniques.

5.2.1 Luminescence based detection of $^{1}O_2$

Yuan and co-workers developed two families of europium probes specific for singlet oxygen (Fig. 10). They are based on either terpyridine ligands (**7**) or β-diketonate (**8**)[119, 120] appended by anthryl moiety. [121-124] The detection method is based on

the reaction of the anthryl group with $^1O_2$, affording an endoperoxide, as depicted in Fig. 10 for **8**.

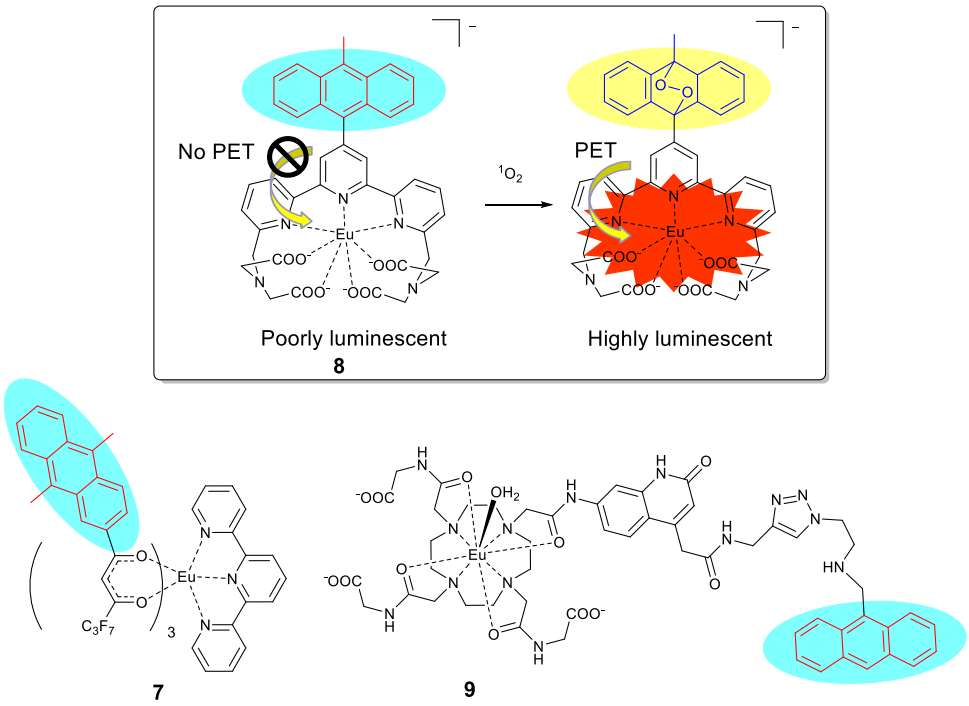

Figure 10. Europium complexes appended by anthryl moiety and designed for singlet oxygen detection; Principle of detection of $^1O_2$.

The Eu^{3+} complex **7** (Fig. 10) [119] was designed for the time-gated luminescence detection of $^1O_2$ in living cells. Furthermore, the mitochondria-targetable feature of the probe was demonstrated by imaging the HepG2 cells coloaded with the probe and Mito-Tracker Green. The initial complex shows a weak luminescence of europium ion due to the strong quenching effect of the anthryl group, which interrupts the intramolecular photoinduced electron transfer (PET). $^1O_2$ specifically reacts with the anthryl moiety, giving an endoperoxide derivative, with subsequent restoration of the PET. The endoperoxide derivative proved to be highly luminescent (quantum yield increasing from Φ = 17.2% to 53.3%). Furthermore, the probe was found to be specific for singlet oxygen among five other ROS/RNS ($ONOO^-$, NO, $OH^\bullet$, H_2O_2 and ClO^-) and selective towards mitochondria.

Some other groups exploited the same anthryl specific detection of singlet oxygen using Nd^{3+} [118] or Eu^{3+}-triazine structures (**9**, Fig. 10) [125]. More specifically the Nd^{3+} triazine complex carried an anthracene moiety and allowed a specific detection of singlet

oxygen specifically in the NIR window. This complex showed an increase of NIR band at 900 and 1075 nm upon titration of singlet oxygen forming the endoperoxide moiety.

5.2.2 ParaCEST based detection of single $^1O_2$

Only a single example of singlet oxygen detection using ParaCEST (Paramagnetic chemical exchange saturation transfer) was reported [126]. Sherry and co-workers designed a DOTA-tetraamide derivative bearing an anthryl moiety **10** (Fig. 11). Before reaction with singlet oxygen, the europium complex exhibited a CEST signal near 50 ppm, typical for an Eu-water exchange peak. Upon reaction with $^1O_2$ and subsequent formation of the endoperoxide, a shift to 53 ppm is observed. in parallel the residual lifetime of the water molecule on the europium ion increased from 90 µs to 137 µs. The difference of 3 ppm between the two forms is sufficient for ratiometric detection in the 0 to 20 mM range. Hence *in vivo* detection is in principle possible, though the high quantity needed for detection by CEST imaging is yet limiting.

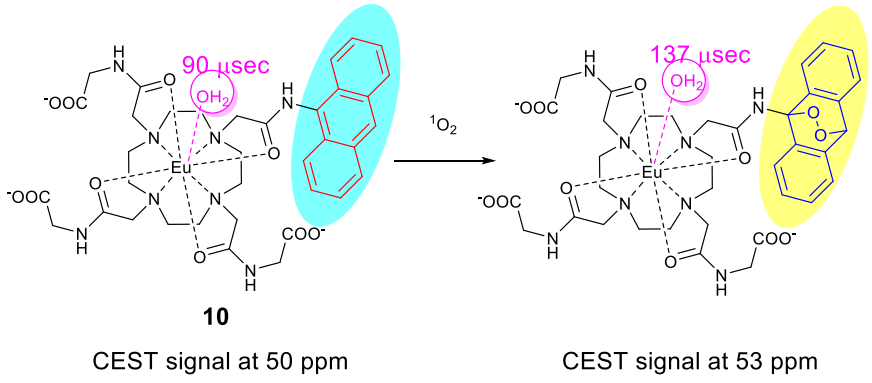

Figure 11. Principle of detection of $^1O_2$ by complex **10**

6. Detection of reactive oxygen species (ROS)

As detailed above, ROS are generated by an incomplete reduction of molecular oxygen. They have a dual role in the body, acting sometime as beneficial species (signalling, defence against pathogens …), but sometime as toxic agents (oxidative stress). Detection of reactive oxygen species allows a better understanding of their formation, control and exact roles. The spectroscopies used for the detection of ROS by lanthanide complexes encompass turn ON/OFF luminescence, EPR, MRI and ParaCEST, the first being the most investigated technique. In the following we will provide an overview of the

methods utilising lanthanide complexes and their redox properties for the detection of reactive oxygen species (Fig. 12). Each ROS will be described in a distinct section due to their strikingly different reactivity and properties (H_2O_2, HOCl, $OH^{\bullet}$), while detection of multiple ROS at the same time will be presented at the end.

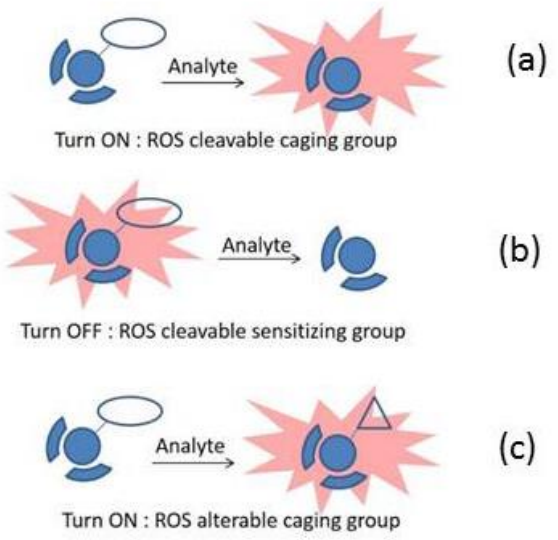

Figure 12. ROS sensitive groups effecting luminescent sensing

6.1 Hydrogen peroxide

Detection of hydrogen peroxide by a simple, fast, low cost and precise manner is an active domain of research. Up to now, many approaches, including chemiluminescence, fluorescence, colorimetric or electrochemical methods have been employed. Few lanthanide complexes were designed to detect H_2O_2. The detection is currently based on luminescence techniques, whereby the irreversible oxidation of the ligand induces the quenching or enhancement of the lanthanide emission (Fig. 12b-c).

6.1.1 Turn ON detection

The ideal scenario for luminescent sensing is a turn ON switch which allows a very definite and easy to detect response (Fig. 12a,c). For such detection the antenna acts as a quencher and no luminescence is observable before addition of ROS. After reaction with H_2O_2 the ligand becomes a better sensitizer, resulting in enhanced luminescence and hence turns ON detection of H_2O_2 (Fig. 12a,c).

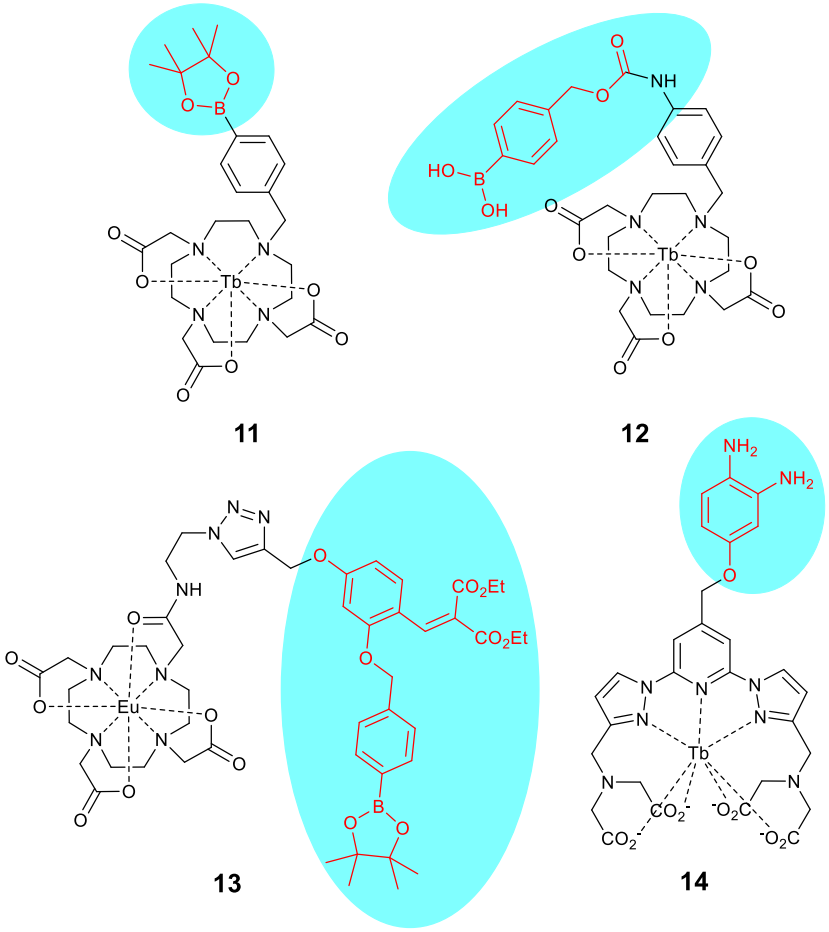

Figure 13. Structure of complexes for switch on detection of H_2O_2.

With this aim Chang and co-workers reported two terbium peroxy reporters **11** and **12** (Fig. 13) whose luminescence could be detected by time-gated luminescence. They were selective towards hydrogen peroxide among seven other ROS [127]. Before reaction, both terbium chelates (**11** and **12**) were weakly luminescent, showing a luminescence lifetime of 1.26 and 1.36 ms and a quantum yield of 2.9 % and 2.6 % respectively. After treatment with hydrogen peroxide, the benzyl boronic acid unit is cleaved, affording a boric diester, 4-methylene-2,5-cyclohexadien-1-one and a newly-formed terbium complex (Fig. 14). The newly-formed terbium complexes showed an increase of the terbium luminescence due to the higher quantum yields of 5.4 % and 5.1 %, respectively. Even if these complexes are non ratiometric, the authors were able to detect an elevation in H_2O_2 production in water and in living cells. Borbas and co-workers reported a series of lanthanide chelates as luminescent probes for detection of various analytes [128, 129].

This was achieved by adding a non-sensitizing antenna precursor appended by a caged benzylboronic acid (selective to H_2O_2) on a DOTA ligand to give **13**. These complexes were almost non-emissive in this caged-form **13**, "OFF" (Fig. 13). After reaction with hydrogen peroxide, coumarin was released (Fig. 14) and the new europium complex displayed a lanthanide luminescence with a quantum yield around 0.31% and a decrease of lifetime luminescence from 1.21 ms to 0.7 ms. Both **13** and its analog terbium chelates show a linear response to hydrogen peroxide concentration in the 0-200 µM range, with a limit of detection calculated at 1 µM.

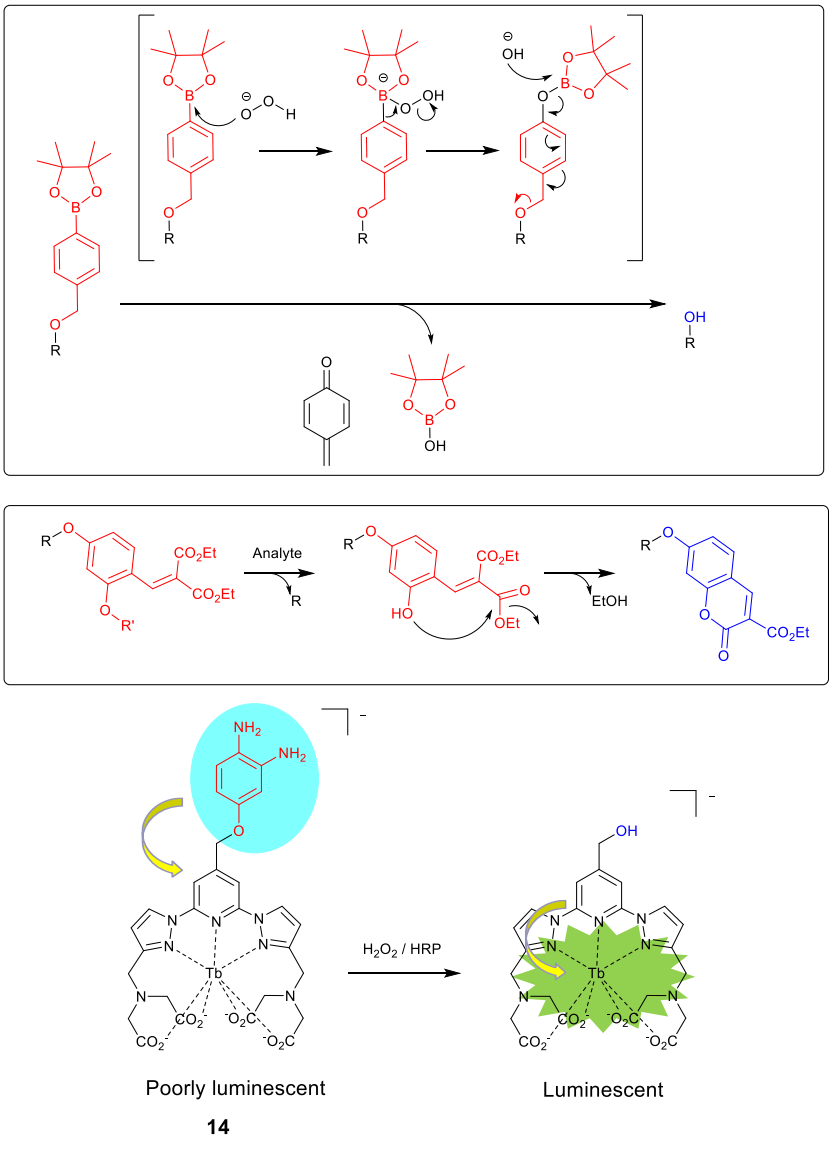

Figure 14. Mechanisms for turn ON detection of H_2O_2.

Yuan and co-workers presented another complex with turn ON type detection [130]. Before treatment with H_2O_2, complex **14** (Fig. 14) showed a weak terbium luminescence

with a quantum yield of 0.20% and a lifetime luminescence of 1.95 ms. The electron rich diaminophenyl moiety strongly quenches the lanthanide luminescence due to a photoinduced electron transfer (PET). After oxidation by H_2O_2 in the presence of peroxidase the ligand is cleaved, the PET is no longer operative and sensitization of the lanthanide is possible (Fig. 14). As a consequence, the complex becomes highly luminescent with a quantum yield of 7.8 %, a long luminescence lifetime of 2.76 ms, and a linear response to hydrogen peroxide concentration in 0.0037-1 µM range.

6.1.2 Turn OFF detection

The switch OFF detection requires a lanthanide complex that is already luminescent. Its oxidation results in an alteration of the antenna with subsequent quenching of the luminescence. Yuan and co-workers reported such a complex (Fig. 15)[131]. Before treatment with H_2O_2, complex **15** showed a high europium luminescence with a quantum yield of 12.1%. After reaction with H_2O_2, the 4-pyridinylboronic acid is converted into deprotonated 4-hydroxypyridine. The resulting complex is non-luminescent due to quenching by an intramolecular charge transfer. This europium chelate showed a linear response to hydrogen peroxide concentration in the 100-1000 µM range.

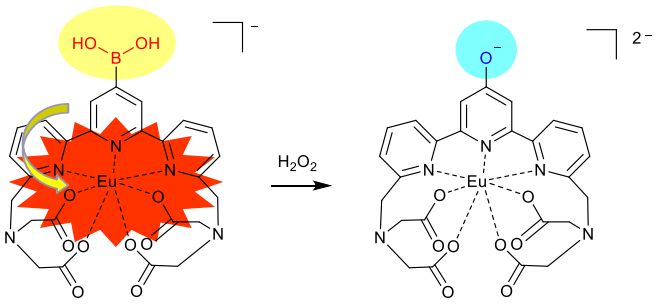

Figure 15. Luminescent switch OFF probe upon reaction with H_2O_2

Zuchner and co-workers[132] presented more recently a simple time-resolved fluorescence assay for the detection of H_2O_2. Phthalic acid and the terbium ion (free metal salt) were mixed together in an optimal ratio of 1:3 in the range of pH 7.0 to 9.0. Without hydrogen peroxide, the quantum yield was around 0.17%. Addition of hydrogen

peroxide caused a linear decrease of fluorescence in very large range from 0.3 to 2560 µM with a limit of detection of 0.15 µM.

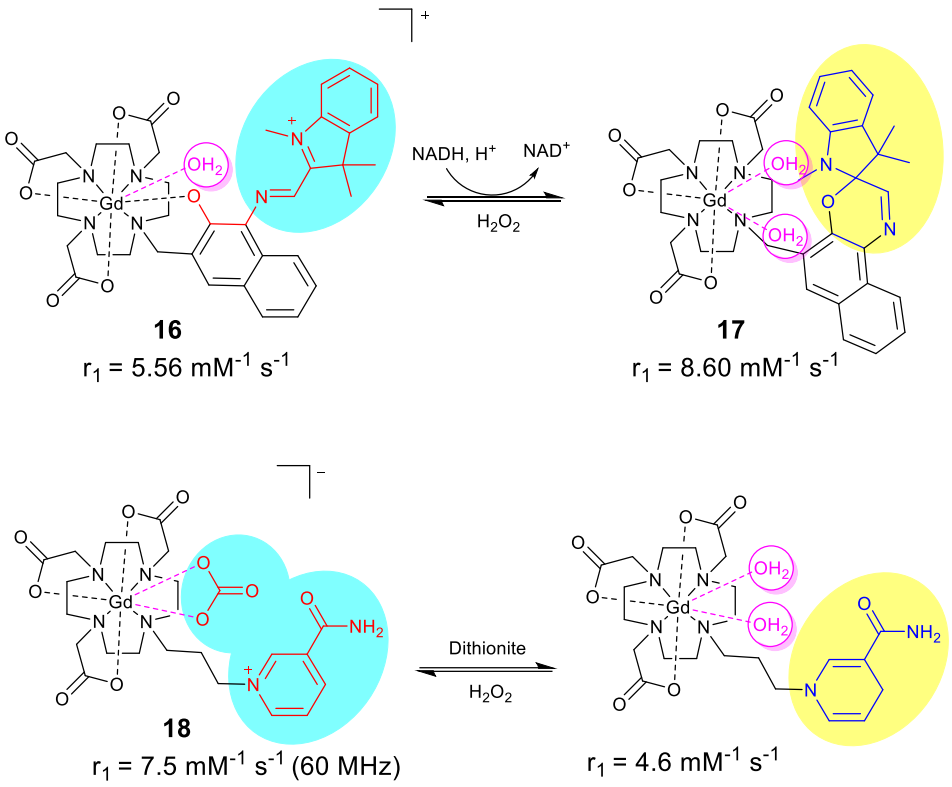

Figure 16. Reaction of **16**-**17** with reductants and H_2O_2

6.1.3 MRI based detection

One example of detection of H_2O_2 by MRI was achieved by using the DO3A platform appended by a merocyanine unit **16** (Fig. 16). Its Gd^{3+} complex could be isomerized into spirooxazine by reaction with NADH, affording **17**. [13] Complex **17** could be partially converted back into the merocyanine complex by oxidation with H_2O_2. The number of coordinated water molecules evolves from 2 to 1 upon oxidation due to the coordination of the pendent arm, with a change in relaxivity from 8.60 (spirooxazine, **17**) to 5.56 $mM.s^{-1}$ (merocyanine, **16**) at 4.7 T. Recently the DO3A platform has been functionalized by a redox-active nicotinamide arm to give complex **18** (Fig. 16) [133]. Under its reduced form complex **18** features two bound water molecules. The addition of H_2O_2 in the presence of bicarbonate (largely present in the blood) changes the overall charge of the complex, inducing the binding of bicarbonate, with release of the water molecules.

This change in coordination is accompanied by a large increase in relaxivity, from r_1 = 4.6 mM^{-1} s^{-1} to 7.5 mM^{-1} s^{-1} at 60 MHz.

6.2 Hypochlorite

Hypochlorous acid is a ROS primarily involved in inflammation processes and immune response. In living systems, endogenous HOCl is produced in a reaction between hydrogen peroxide and chloride ions catalysed by myeloperoxidase. The quantitative detection of hypochlorous acid in living systems by lanthanide probes has been developed recently. It currently employs exclusively luminescence spectroscopy. In this section we provided an overview of the two main types of probes (turn ON and OFF) that use lanthanide complexes and their redox properties for the detection of hypochlorous acid.

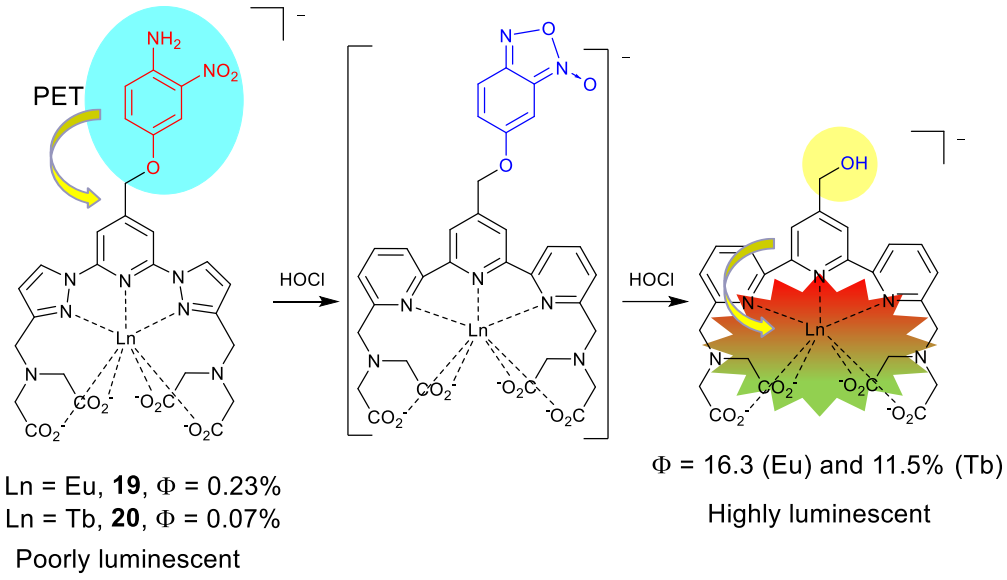

Figure 17. Reaction of **19** and **20** with HOCl

6.2.1 Turn ON detection

The first strategy to obtain a turn ON specific detection of HOCl is based on a photo-induced electron transfer. Yuan and co-workers investigated five complexes wherein the lanthanide luminescence is modulated with PET mechanism [134, 135]. Complexes **19** and **20** (Fig. 17) show a weak luminescence with quantum yields of 0.23 and 0.07%, respectively [136]. The lanthanide luminescence is indeed quenched by a PET from the

4-amino-3-nitrophenyloxy moiety to the terpyridine. After treatment with HOCl an oxidative cleavage is observed, with release of benzoxadiazole by-product and an elimination of the PET effect. The resulting europium and terbium complexes are highly luminescent, with quantum yields of 16.3 and 11.5%, respectively. These complexes allowed *in vivo* detection of HOCl in a range 0.01-1 µM, with detection limit of about 1 nM.

Complex **21** (Fig. 18) allows for the detection of HOCl according to an intramolecular Förster resonance energy transfer (FRET) mechanism. It associates a luminescent terpyridine polyacid terbium complex (FRET donor) and a rhodamine moiety (FRET acceptor) [137]. In the absence of HOCl, the rhodamine moiety adopts a spirolactam form that quenches the FRET acceptor capability. The observed luminescence is only due to the Tb^{3+} emission. After reaction with HOCl, the spirolactam is decomposed and the free rhodamine can act as a FRET acceptor. The FRET from the terbium ion to the rhodamine moiety is restored, resulting in an increase of the ratio of emission I_{560}/I_{540}.

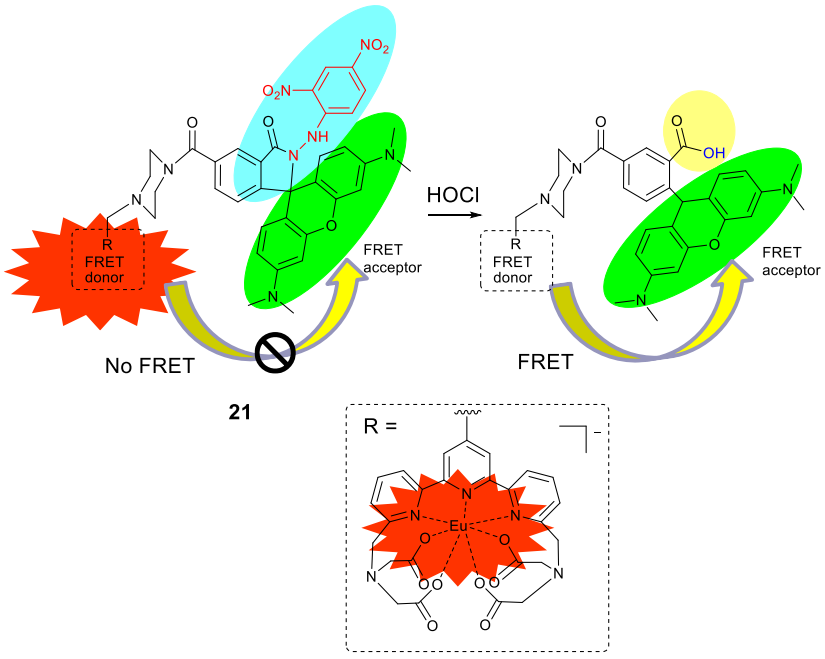

Figure 18. FRET mechanism between a luminescent terbium complex (FRET donor) and a rhodamine moiety (FRET acceptor)

6.2.2 Turn OFF detection

Two β-diketonate-Eu^{3+} complexes, **22** and **23**, were developed by Yuan and co-workers for the turn OFF detection of HOCl (Fig. 19). These complexes are appended by triphenylphosphonium and morpholine groups, respectively, which allow for targeting mitochondria and lysosomes.

Complexes **22** and **23** (Fig. 19) were designed for a time-gated luminescence imaging of HOCl in living systems. Both complexes showed a high quantum yield (56.8% and 46.2% respectively). After reaction with HOCl, the carbonyl groups of the β-diketonate moieties are oxidized into carboxylic acids. The europium complexes are next decomposed, resulting in a quenching of the luminescence. Sorensen and Giorgio recently reported some other complexes based on DO2A and DO3A platforms, all appended with a hydroquinone caging moiety (complexes **24** and **25** in Fig. 19 belong to this series)[138]. Upon reaction with HOCl, the hydroquinone cage is released and a symmetrical and simple [Ln.DOTA]$^{-}$ complex forms. This transformation can be followed both by luminescence and NMR spectroscopy. However, none of the complexes of this latter series incorporates a chromophore, which limits their application as biological luminescent probes.

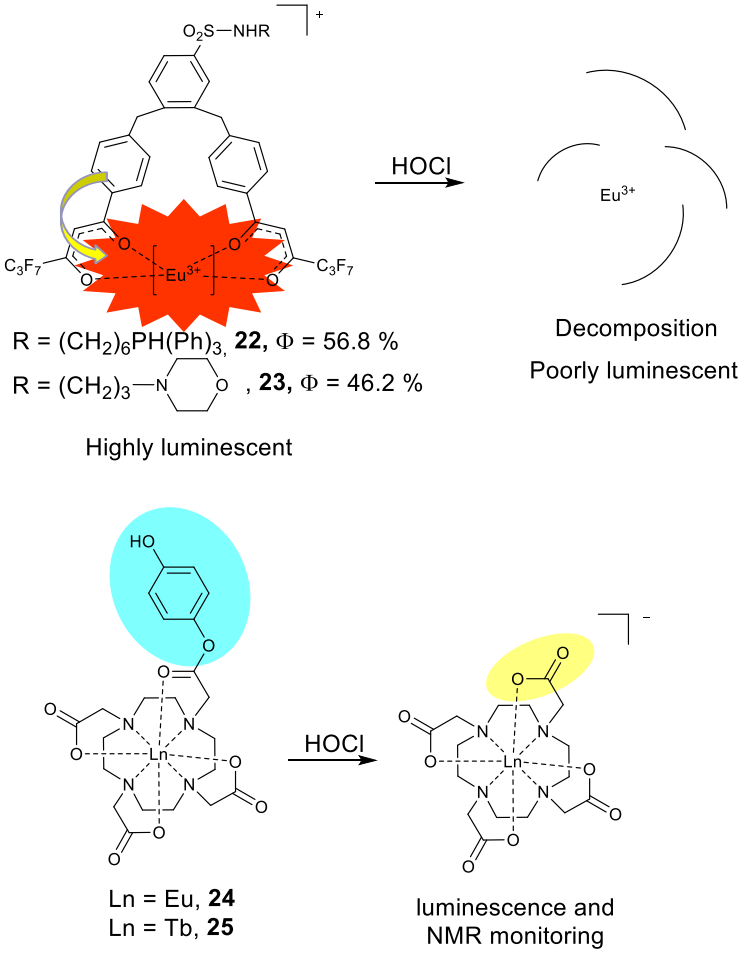

Figure 19. Complexes for turn OFF detection of HOCl

6.3 Hydroxyl radical

The hydroxyl radical HO• is the most reactive ROS, with a lifetime in the nanosecond range. This reactive species plays an important role in a variety of physiological processes, while being the most harmful ROS [139]. Only a few lanthanide complexes allow for selective detection of the hydroxyl radical using either luminescence or bimodal EPR/ luminescence methods. The methods exploit the high reactivity of the HO• radical to chemically modify the probe and subsequently its properties. In contrast to H_2O_2, whose ability to form endoperoxides with the anthryl group only has been exploited, a wider range of reactivities with HO• has been investigated.

6.3.1 Turn ON detection

Pierre and co-workers described a turn ON system based on both a terbium DO2A or DO3A (**26**, Fig. 20) and an aromatic pre-antenna (benzoate, benzamide, isophthalate, isophthalamide, trimesate or trimesamid) [140, 141]. The pre-antenna does not sensitize the terbium ions and likely does not coordinate. It gets hydroxylated in the presence of hydroxyl radicals, affording a good and selective antenna, which is proposed to interact via second-sphere effect or displacement of one carboxylate of the macrocycle. Sensitization is achieved by shifting the antenna triplet excited state slightly above the $^5D_4$ excited state of Tb and a diminution of lanthanide to antenna distance. The trimesamide/**26** system undergoes a 1000-fold enhancement of metal-centered time-delayed emission, which enables a very sensitive detection of HO•.

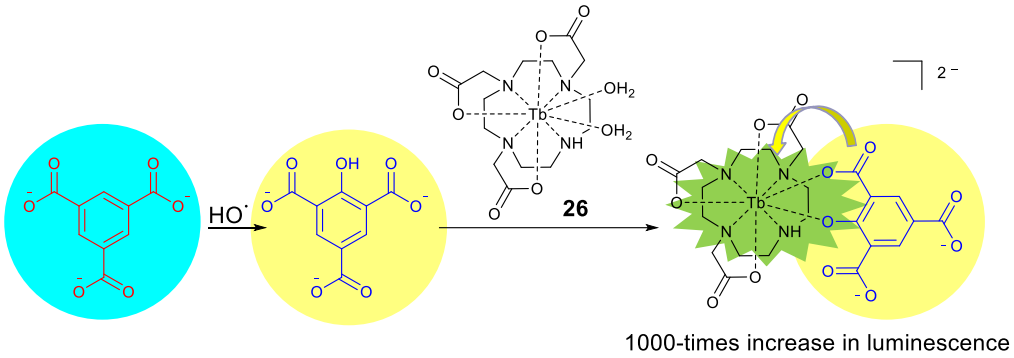

Figure 20. Turn ON system based on both the terbium complex **26** and an aromatic trimesate pre-antenna

6.3.2 Bimodal (EPR and luminescence) detection

The bimodal detection (EPR/luminescence) of HO$^{\bullet}$ requires formation or disappearance of a radical-containing lanthanide probe. Guo and co-workers reported the first example of spin-labelled lanthanide complexes for detection of HO$^{\bullet}$ with a limit of detection of 4 nM. The spin-labelled terbium complex **27** (Fig. 21)[142] combines both a fluorophore and a nitroxide radical on an acyclic DTPA ligand. Before reaction with HO$^{\bullet}$, the complex exhibits a characteristic three-line pattern centered at g = 2.006 in its EPR spectrum. It is not luminescent because the paramagnetic nitroxide moiety quenches the excited state of fluorophore. Detection of the hydroxyl radical is based on the propensity of HO$^{\bullet}$ to react with DMSO (solvent), affording primarily a carbon centred radical $CH_3^{\bullet}$. In a second step the methyl radical reacts irreversibly with the nitroxyde moiety to give the diamagnetic alkoxyamine derivative. As a result, the TEMPO resonances disappear from the EPR spectrum. Conversely the diamagnetism of the ligand does not quench the luminescence, resulting in a turn ON detection.

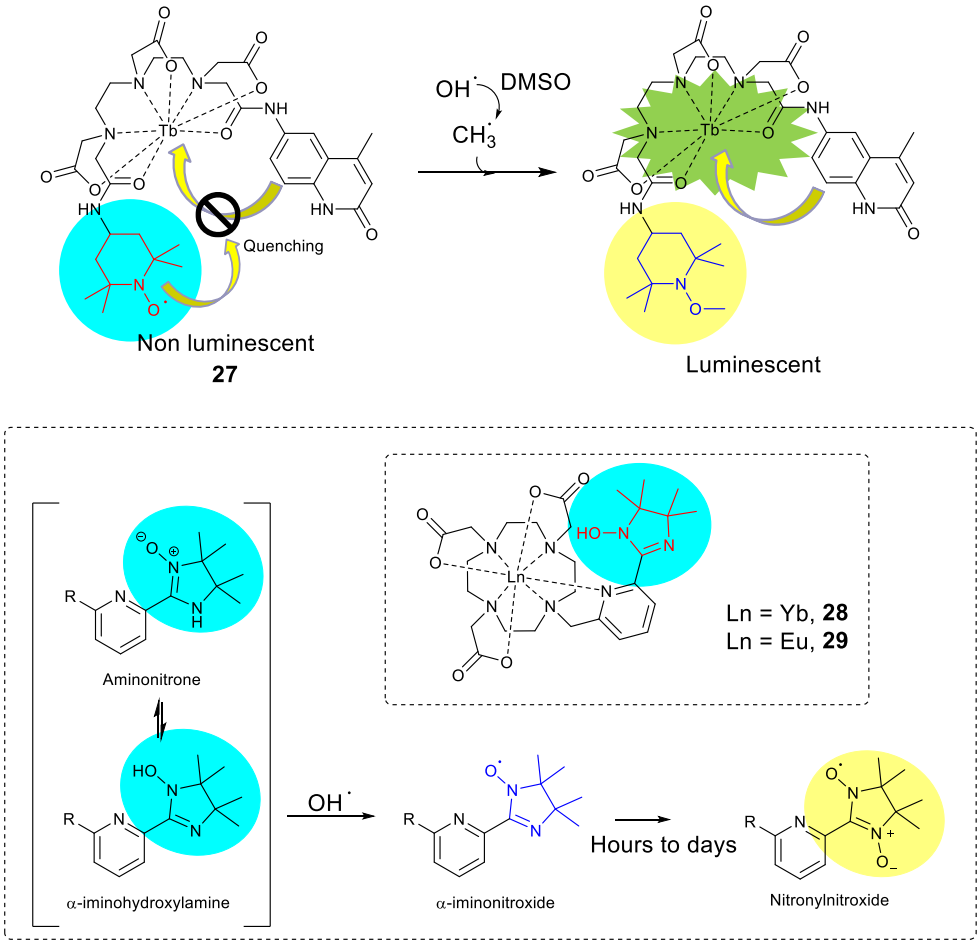

Figure 21. Detection of OH• by reaction with a pro-nitroxide unit

More recently, we reported luminescent europium and ytterbium complexes based on a DO3A ligand appended by a pyridine-α-iminohydroxylamine (**28**-**29**, Fig. 21) [143]. Upon reaction with HO•, the α-iminohydroxylamine is converted into the paramagnetic α-iminonitroxide moiety after few hours and evolved into the violet nitronyl-nitroxide radical after 2-6 days. The reaction could be readily monitored by EPR spectroscopy by the appearance of a 1:1:2:1:2:1:1 signal that further disappears at the expense of a new 1:2:3:2:1 signal. The formation of the new paramagnetic species is associated to a quenching of the luminescence by 15 to 28% (**28** and **29**, respectively).

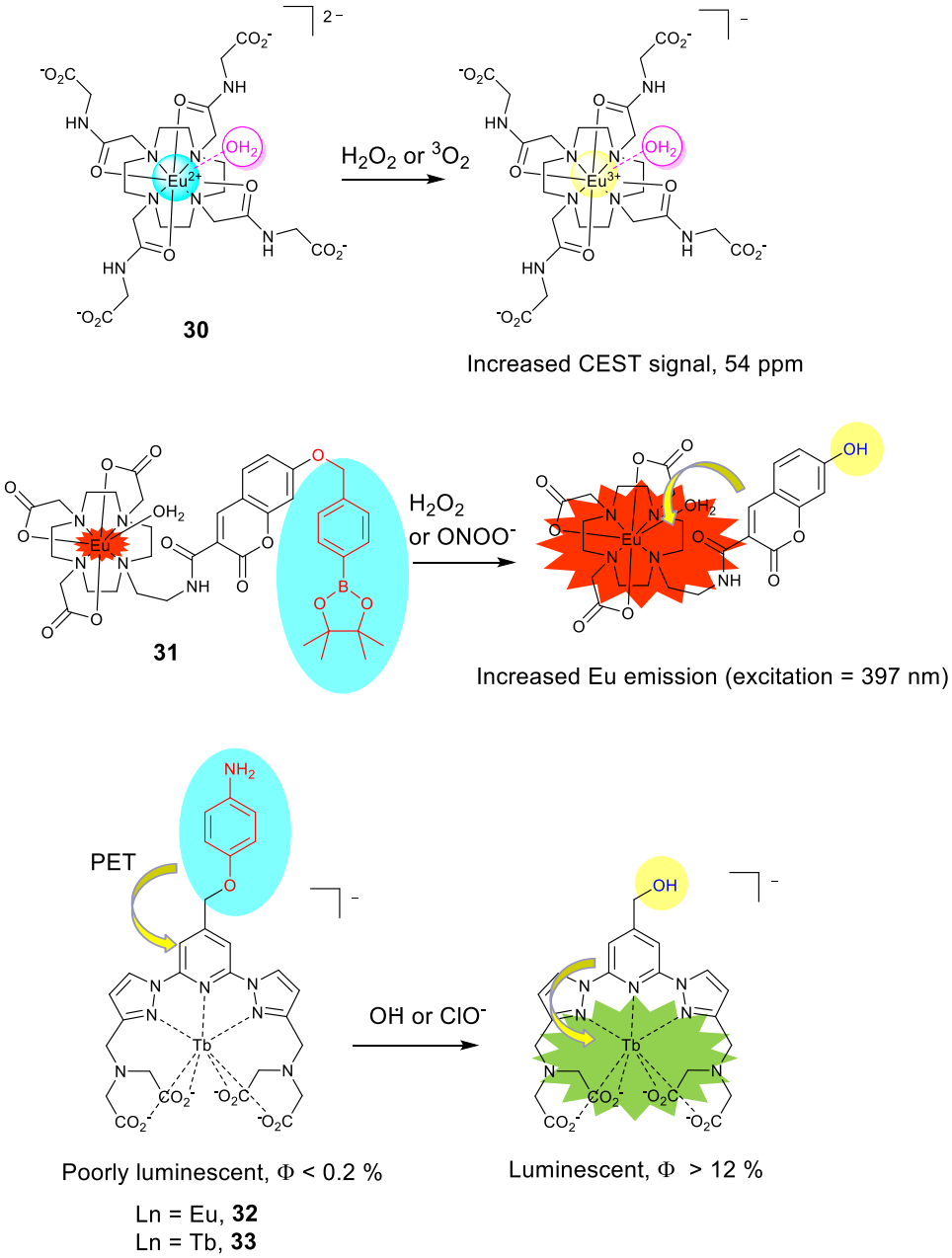

Figure 22. Detection of multiple ROS by lanthanide complexes

6.4 Multiple ROS at the same time

Some complexes were shown to react with several ROS, allowing for a global response [85, 144] [145, 146].

The first example is a bimodal europium probe **30** (Fig. 22) developed by Kovacs and co-workers.[85] Divalent Eu^{2+} is isoelectronic with Gd^{3+}, with comparable r_1 relaxivity and can be detected by MRI. Due to a strong negative reduction potential of -0.59 V (vs Ag^+/Ag), Eu^{2+} can be oxidized by $^3O_2$ or H_2O_2 into Eu^{3+} which is no longer an efficient

T_1 shortening agent. The resulting complex has a hyperfine shift effect on water proton detectable by ParaCEST at 54 ppm. The probe could be followed *in vivo* by both techniques in order to map a redox environment. Complex **31** (Fig. 22) reacts both with H_2O_2 and ONO_2^- (see below), albeit faster in the second case. The mechanism is identical to that depicted in Fig. 14, whereby the aryl boronate cage is oxidized and released, affording a 7-hydroxycoumarin appended complex. Sensitization is changed and an increase in the Eu^{3+} luminescence is observed upon excitation at 397 nm. The complexes **32-33** (Ln = Eu^{3+}, Tb^{3+}) are derived from **14** (Fig. 14), but differ by the presence of an aminophenyl instead of diaminophenyl group. They are almost nonluminescent ($\Phi < 0.2$ %) due to the PET from this electron-rich group to the Ln(terpyridine) unit. They readily react with both $OH^{\bullet}$ and ClO^-, resulting in an uncapping of the ligand and further quenching of the PET. The complexes become highly luminescent ($\Phi > 12$ %), with an increase of luminescence lifetimes. By using an equimolar mixture of **32** and **33**, and following the ratio of the intensity of emission I_{540}/I_{610} (Tb^{3+} and Eu^{3+} emission maxima, respectively) a ratiometric response was obtained.

7. RNS detection

Reactive nitrogen species (RNS) refers to a family of small reactive molecules whose actors are nitric oxide (NO), and mainly peroxynitrite (ONO_2^-). NO is a weak oxidant, while peroxynitrite is a reactive peroxide whose half-life at pH 7.4 and 37 °C in phosphate buffer is about 0.6 s (less than 20 msec within the cell). In spite of this order of reactivity, a chemical reaction of NO with the probe will be employed for its detection, whereas either chemical reaction or simple interaction will be the basis for the detection of peroxynitrite.

7.1 Nitric oxide

The development of NO responsive lanthanide probes is based on two different strategies: ratiometric time gated luminescence measurements (TGLM) and paraCEST measurements. In both cases, a chemical function is used to trap NO, leading to a change in the properties of the complex, either luminescence intensity, luminescence lifetime or paraCEST signal.

7.1.1 Luminescence-based detection

Only a few luminescence-based probes were designed for NO detection (Fig. 23-24). The first example reported by Yuan's group is the Eu^{3+} complex **34** bearing an electron rich *o*-diaminophenyl group [147]. This moiety is known to quench efficiently the luminescence by PET. After reaction with NO under aerobic conditions, the *o*-diaminophenyl group undergoes a cyclisation to form the corresponding benzotriazole derivative, which enables Ln sensitization and leads to a luminescence turn ON with a 47-fold increase at physiological pH (Fig. 23). The detection limit for NO is 8.4 nM. The selectivity of complex **34** was investigated against nine ROS and RNS. It was found to be very remarkably specific for NO, especially against $ONOO^-$.

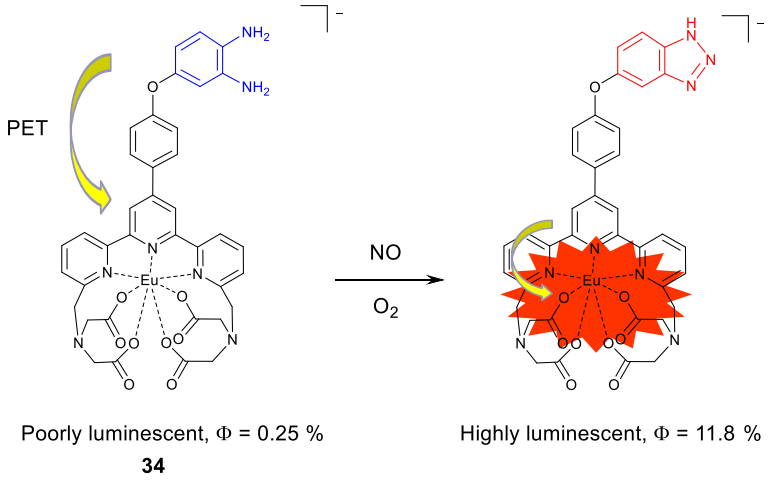

Figure 23. Turn-on NO detection mechanism based on the quenching of a photo-induced electron transfer process.

Four years later, Yuan's group published another luminescence-based probe (Fig. 24), this time based on a luminescence resonance energy transfer (LRET) process, between a Tb^{3+} complex **35** and a rhodamine derivative (**Rh-NO**) [55d]. To ensure the proximity of these two units, Yuan and co-workers used apoferritin (AFt) as carrier. This protein is known to enable encapsulation of complexes or nanoparticles for imaging purposes [56]. In this LRET probe, **35** is encapsulated in the core of apoferritin as the energy donor, affording **35**@AFt-**Rh-NO**. **Rh-NO** which is both the energy acceptor and the NO sensitive unit, is bound to the surface of apoferritin. As a result, in the absence of NO, only the strong Tb^{3+} luminescence is observed. Upon reaction with NO, rhodamine luminescence is switched-on with the LRET process and Tb^{3+} luminescence is turned-OFF.

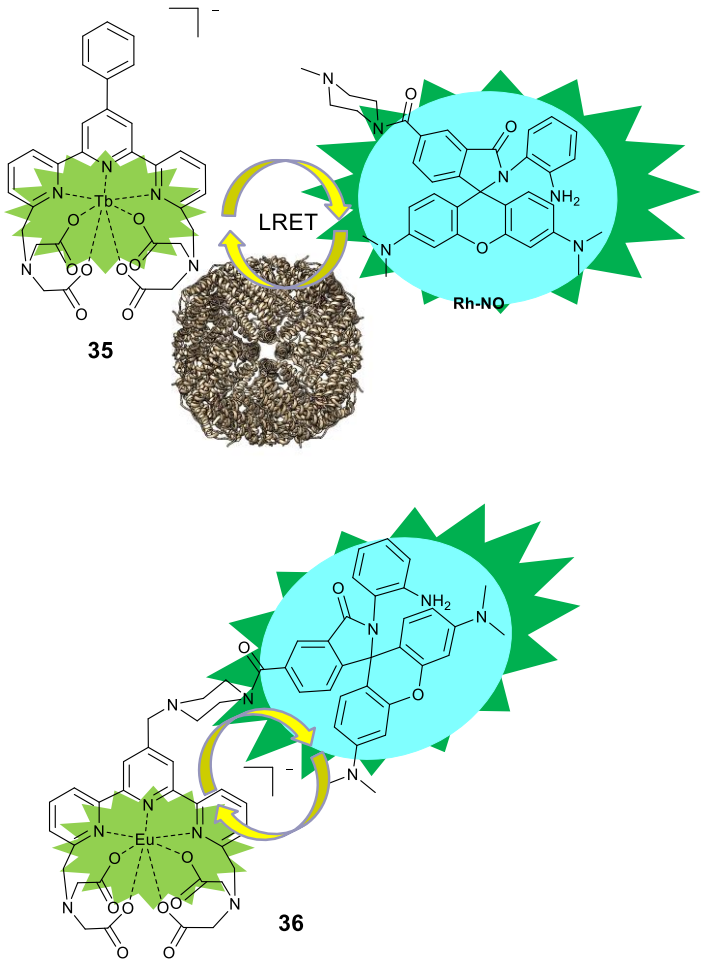

Figure 24. Luminescent lanthanide probes for NO detection. [55a,b,c,d] LRET: luminescence resonance energy transfer.

The LRET process greatly depends on the spectral overlap of the donor and acceptor. The luminescence of **35** reaches a maximum at 539 nm corresponding to the $^5D_4 \rightarrow {}^7F_5$ transition. **Rh-NO** has a maximum emission at 577 nm but in order to obtain a ratiometric measurement, the luminescence intensity need to be taken at 565 nm, where luminescence of **35** is almost silent while the rhodamine still has 90% of its maximum intensity. The LRET process efficiency (E) was calculated and found to be 77.8%. It was calculated with the following equation [145]:

$$E = 1 - \frac{\tau_{AD}}{\tau_D}$$

with τ_D (331.3 μs) the lifetime of the donor without the acceptor and τ_{AD} (73.7 μs) the luminescence lifetime of the donor with the acceptor. This result confirms the potential of this system for NO detection by TGLM. To evaluate its practical applicability for the

ratiometric time-gated luminescence imaging of NO in living samples, the **35**@AFt-**Rh-NO**-loaded HepG2 cells (Fig. 25) were prepared, and images of the samples in the absence and presence of NO were recorded both under steady-state and time-gated imaging modes [148]. In the absence of NO, Tb^{3+} green luminescence can be well observed but rhodamine luminescence is not observable. After reaction with NO, rhodamine red-luminescence is well observed while Tb luminescence seems to diminish. Two years later, Yuan's groups developed a molecular version of this LRET system by combining the donor and acceptor on a single molecule **36** (Fig. 24). Complex **36** reacts with NO, with the release of a benzotriazole molecule [148]. In this complex, as the donor and the acceptor are covalently bounded, the efficiency of the energy transfer is higher compared to the previous one (98.5%, with τ_D = 1.1 ms, τ_{AD} = 16 μs). The measured ratio between Tb^{3+} and rhodamine luminescence intensities I_{565}/I_{540} is in the same range than the apoferritin platform (28.8). Interesting features are observed regarding the luminescence lifetime of the probe. As it is greatly influenced by the intramolecular LRET, the authors recorded the luminescence lifetime of **36** with different NO concentrations. The lifetime of the probe gradually decreases from 484.3 μs to 48.7 μs upon reaction with NO. Luminescence lifetimes can thus be used as a modality for NO imaging with a 10-fold contrast window. The effects of nine different ROS and RNS on the I_{565}/I_{540} ratio and the luminescence lifetime of **36** were investigated and selectivity towards NO was found to be remarkable.

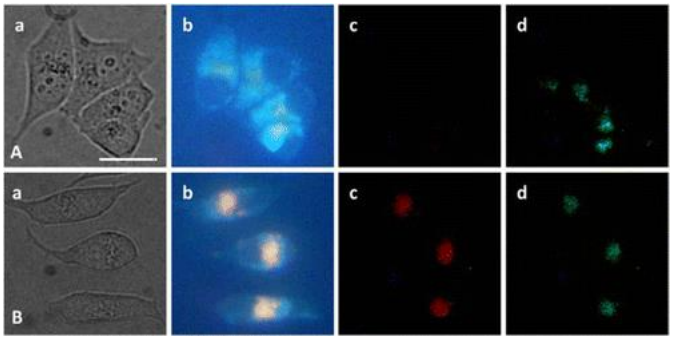

Figure 25. Ratiometric TGL imaging of NO in HepG2 cells by using the Apoferritin-assembled **35@AFt-Rh-NO** FRET system. (a) Bright-field; (b) steady-state; (c,d) time-gated (red filter, >590 nm, for collecting rhodamine luminescence signals and green filter, 540 ± 25 nm, for collecting Tb^{3+} luminescence signals, respectively) luminescence images before (A) and after (B) reaction with NO. Scale bar: 10 μm.

Reprinted with permission from L. Tian, Z. Dai, X. Liu, B. Song, Z. Ye, J. Yuan, Anal. Chem., 87 (2015) 10878-10885 [148]. Copyright 2015 American Chemical Society.

7.1.2 MRI and paraCEST-based detection

Chemical exchange saturation transfer (CEST) MRI is an alternative to the classical relaxation-based mechanism. Pagel and coworkers reported in 2007 the first PARACEST agent responsive to NO radicals [149]. The CEST spectra of the complex **37** (Fig. 26) before reaction with NO, shows two peaks at -11ppm and 8ppm, for the amide and amine functions, respectively. After reaction with NO and O_2 the irreversible disappearance of these two signals was observed with the conversion to the triazene. This change is assigned to an irreversible covalent change through endogenous autooxidation of the nitric oxide in the presence of O_2 (Fig. 26)**.**

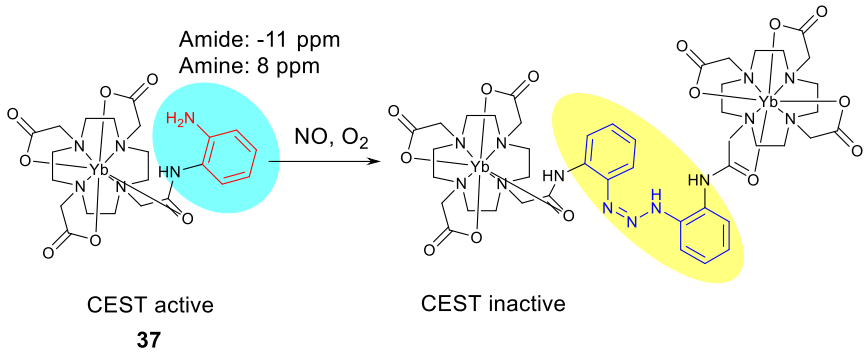

Figure 26. Reaction of **37** with NO in the presence of oxygen that converts aromatic amines to a triazene and further dimeric complex.

7.2 Peroxynitrite

Probes for peroxynitrite typically employ luminescence as a detection technique. They are based on a turn-off detection via either exciplex formation or chemical modification of the probe by reaction with ONO_2^-. Interestingly, peroxynitrite mostly reacts with thiols and phenols within the cell, [42] but none of these reactivities will be used for its detection. In the early 2010 Guan et al. reported europium and terbium complexes based on a polyacid-terpyridine scaffold appended by an electron-rich dimethoxyphenyl group (**38** and **39**, respectively) [150]. Both are luminescent due to efficient sensitization of the lanthanide, with

quantum yields reaching 10%. The luminescence of **38** is not affected by the presence of ONO_2^-, whereas that of **39** is. LC/MS experiments confirm that the ligand remains unchanged in the presence of ONO_2^-. Hence the quenching likely occurs by a charge-transfer mechanism, whereby the electron-rich quenching species interacts with the excited chromophore (exciplex formation). This distinct quenching allows for the design of a ratiometric luminescence probe for time-gated luminescence detection of ONO_2^- simply by mixing the terbium and europium complexes. This probe was proven to be very efficient for the cellular imaging of ONO_2^- in Hela cells.

Wu et al. developed complex **40** (Fig. 27) which associates a bis(pyrazolyl)-1,3,5-triazine–Eu^{3+} unit with a 2,4-dimethoxyphenyl-derived β-diketone ligand [151]. This complex is highly luminescent, as demonstrated by a quantum yield of 64.2 % in the Eu^{3+}-centred emission. The specific interaction between 2,4-dimethoxyphenyl and ONO_2^- causes the quantum yield to drop to 5.3 %, with significant shortening of the luminescence lifetime. Luminescence quenching is proposed to occur via deactivation of the excited states of 2,4-dimethoxyphenyl-substituted lanthanide complexes by ONO_2^- in an exciplex-involved charge-transfer mechanism. A good linear correlation was obtained between the time-gated luminescence intensity and the ONO_2^- concentration in the 5–60 μM, which is within the physiological concentration range of peroxynitrite. Finally, the complex demonstrated low cytotoxicity and was found to be efficient for imaging intracellular ONO_2^-. One year after the same authors reported the terpyridine derivative **41**, which demonstrated the same behaviour [152], with some difference in the quantum yield (25.6 % before reaction with ONO_2^- and 6.7 % after).
A time-resolved ratiometric nanoprobe was designed in 2019 [153]. It comprises the donor unit $Tb(dipicolinate)_3$ which transfers its energy to a receptor unit (DC). The probe emits only the luminescence of DC at 620 nm. After reacting with ONO_2^-, the luminophore DC undergoes chemical transformation, producing an olefine acid product. The energy transfer is no longer possible and only the luminescence of Tb^{3+} can be observed at 547 nm. This results in an enhancement of the intensity ratio I_{547}/I_{620} of 48.7. This nanoprobe was further employed inA-375 cells for sensing endogenous ONO_2^- in mitochondria.
Very recently the europium complex **42** (Fig. 27) is based on a DO3A platform and features a benzyl boronic acid group [154]. It displays a strong Eu^{3+} centred luminescence with a quantum yield of 10%. The benzyl boronic acid reacts rapidly and

selectively with ONO_2^- via oxidative cleavage, affording an 8-hydroxyquinoline unit. This reaction is associated to a significant quenching in luminescence due to the low-lying excited state of the 8-hydroxyquinolinate, which prevents an efficient population of the Eu^{3+} excited state through energy transfer. This complex was cell-permeable and demonstrated to respond to increases in the cellular ONO_2^- levels.

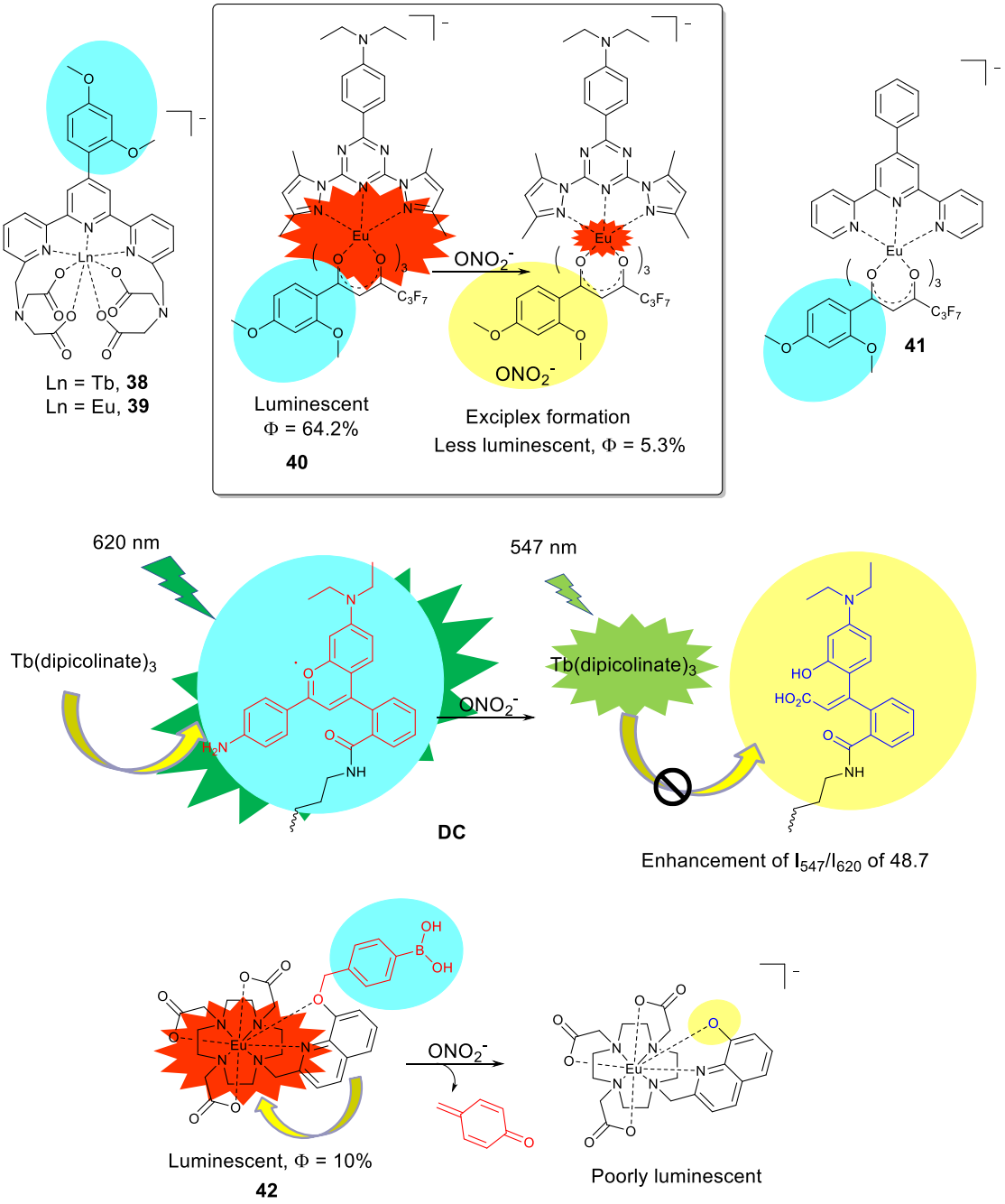

Figure 27. Luminescent lanthanide probes for the detection of peroxynitrite

8. Thiol sensing

The role of sulphur based compounds as redox markers in living organisms has been increasingly studied due to the importance of glutathione as cellular redox buffer [155]. Other important thiols are those found in exofacial proteins located at the extracellular surface of cells, which may act as sensors of the redox state [156]. Yet in connection with the redox balance, protein thiols are known to be very sensitive to ROS [40]. Lastly, H_2S is a potential gaseous transmitter in biological systems, which can be produced *in vivo* from cysteine, homocysteine and cystathionine. High concentrations of H_2S or its conjugated base HS^- have been linked to various diseases such as hypertension, pancreatic or even cancers [157, 158]. Hence the detection of thiols has implications in medical fields, including measurement of the redox status. Two main strategies were employed with distinct detection: One is the generation of higher molecular weight compounds through disulphide bond formation and further detection by MR techniques. The other is a perturbation of the sensitizing process through either chemical alteration of the ligand or coordination to copper (which is known to react with sulphides) and subsequent detection by luminescence.

8.1 Detection of thiols through the thiol/disulphide conversion

The gadolinium complex **43** associates a DOTA platform and a pendent thiol group. It can form a disulphide -S-S- bond with a specific cysteine (Cys34) of human serum albumin [159]. The increase in molecular weight induces a lowering of the tumbling rate, itself inducing an enhanced r_1 relaxivity of the gadolinium complex (5.3 vs 2.33 mM^{-1} s^{-1} at 4.7 T). The extracellular redox status was found to affect the thiol vs disulfide ratio. This property was exploited to monitor the tumor redox status by MRI on tumor xenographs treated with either a glutathione synthesis inhibitor or the thiol-oxidizing anticancer drug Imexon [160]. Using a related approach, the gadolinium complex **44** was designed for reacting with exofacial protein thiols (EPTs). Upon formation of a disulphide bridge complex **44** penetrates the cells and accumulates inside [161]. A correlation was established between the amount of complex inside the cells and the redox state of the EPTs. Further *in vivo* studies on tumor xenografts demonstrated that tumors could be labelled by complex **44** following its direct injection into the tumor [162].

A further example of thiol/disulphide route for redox monitoring is the nanocapsule reported by Botta et al. [163], which was assembled from oxidized thiolated β—cyclodextrins and incorporates complex **45**. Under reducing conditions, the inter β-cyclodextrin disulphide bridges are cleaved and the nanocapsule is destroyed, resulting

in the release of complex **45**. The relaxivity of **45** is dramatically affected, shifting from 19.3 mM^{-1} s^{-1} in the inclusion complex to 7.3 mM^{-1} s^{-1} (at 4.7 T) for free **45** due to its enhanced mobility.

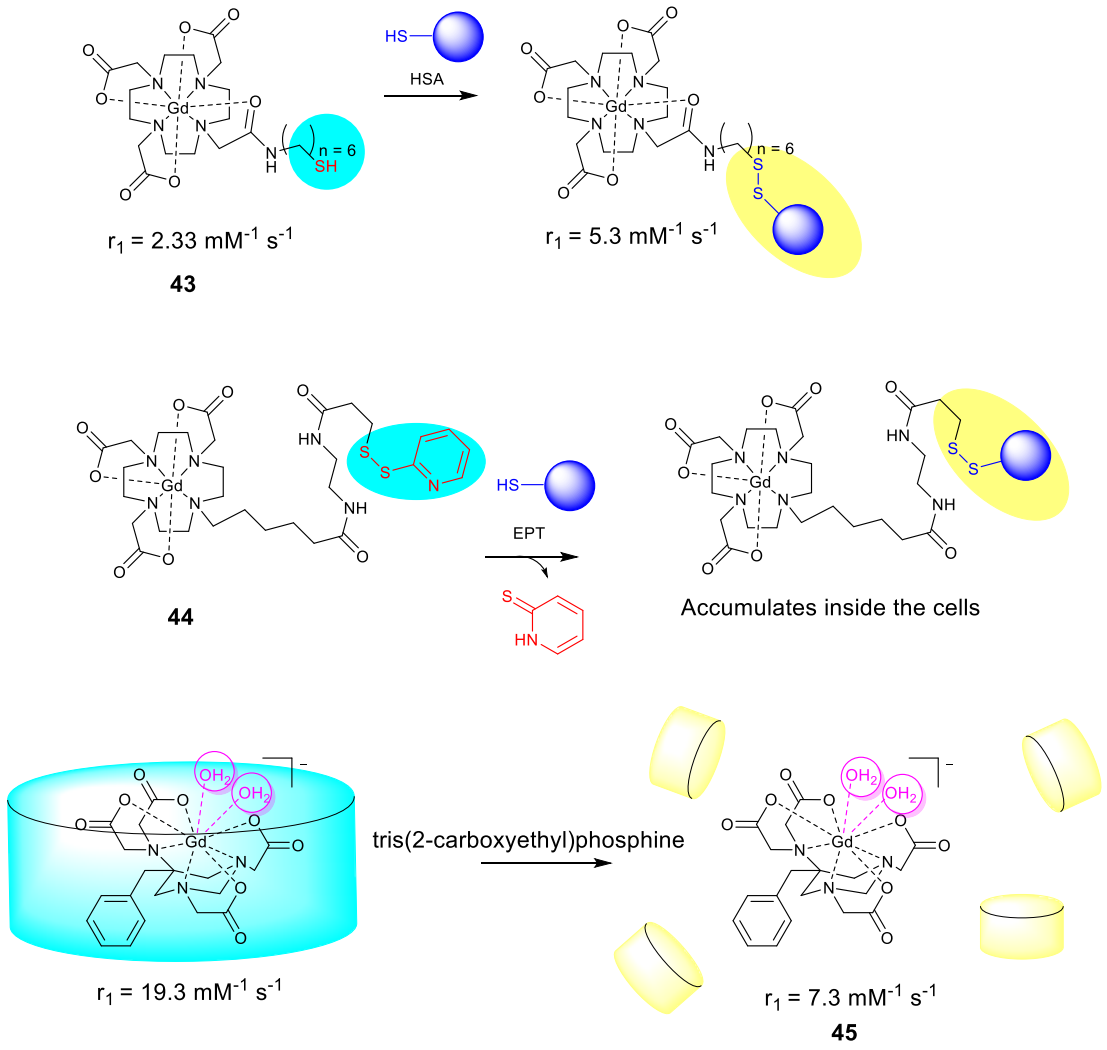

Figure 28. Lanthanide probes for the detection of thiols by magnetic resonance

8.2 Detection via chemical modification

Direct reaction of functionalised europium complexes with sulfide derivatives has been reported to lead to luminescence-based detection of H_2S or HS^-. One of the first examples of a kinetically stable complex which allows time-gated luminescence detection of sulphide was reported is **46** (Fig. 28) [164]. This complex contains a DOTA cage and an aromatic azide arm which can be selectively reduced by H_2S causing

detection via changed energy transfer between antenna and lanthanide ion. This led to 20-fold increase in the luminescence and thus a switch ON signal due to higher charge transfer character. This approach was utilised by another group in parallel to probe sulphide levels in industrial samples [165]. In this case the same design gave similar results, whereby an acetamide linker gives an increase in luminescence. Conversely, the incorporation of a simple CH_2 linker causes a decrease in luminescence upon interaction with H_2S.

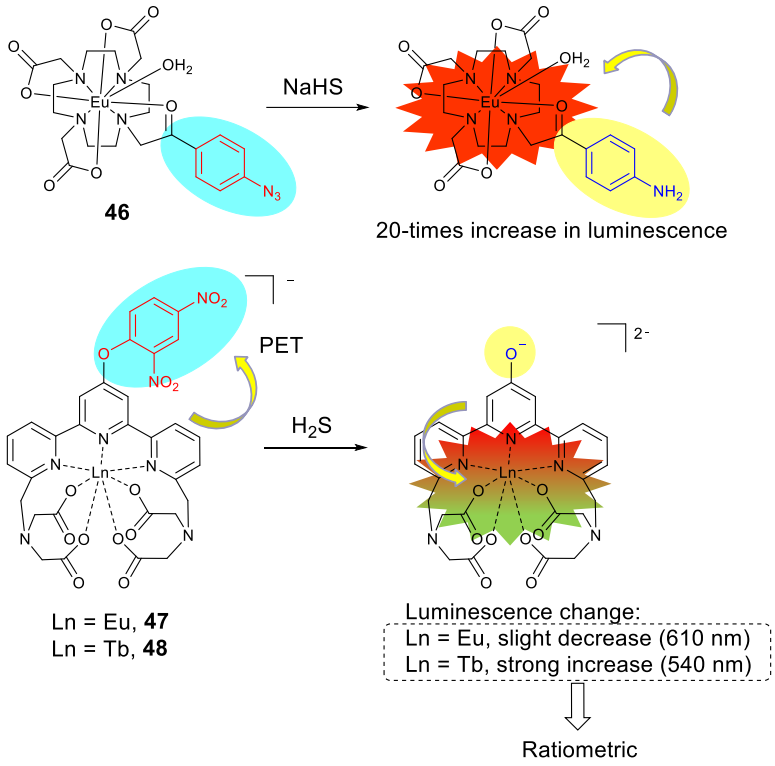

Figure 29. Chemical modifications of complexes **46-48** by NaHS or H_2S that lead to an increase in luminescence (switch ON).

Acyclic complexes based on aromatic moieties capable of cleavage under treatment with H_2S have been developed in the Yuan group [166]. The authors synthesised a weakly luminescent heterobimetallic complexes **47**, **48** based on a terpyridine platform appended by a dinitrophenyl moiety (Fig. 29). Upon reaction with H_2S the dinitrophenyl moiety is cleaved, making the PET no longer effective. The intensity of the Tb^{3+} emission (540 nm) increases remarkably, whereas that of the Eu^{3+} emission (610 nm) is slightly decreased. A ratiometric time-gated detection for H_2S was further demonstrated

using **47**/**48** loaded HepG2 cells and exogenous H_2S imaged using a time gated luminescence microscope.

8.3 Detection via copper coordination

A bis(diketonate) europium complex **49** was designed for the complexation of Cu^{2+} and sulphide ions (Fig. 29) [167]. The probe was strongly fluorescent with a high quantum yield Φ = 57 %. Coordination of Cu^{2+} in the bis[(2-picolyl)amine] unit moiety causes the emission at 607 nm to be almost completely quenched. A complete recovery of the emission is observed after addition of sulphide ion. This change is associated to copper release due to the strong affinity of sulphide with this metal ion (Fig. 30). Yuan et al later demonstrated **50**-**51** (Fig. 30) could be efficiently used as a H_2S detector, by using the same mechanism [168]. Coordination of copper to the bis[(2-picolyl)amine] unit induces a quenching of the Eu^{3+} luminescence. Upon treatment with H_2S copper is released, resulting in a strong enhancement of the Eu^{3+} emission (610 nm), while that of Tb^{3+} does not change significantly. Hence, ratiometric detection is possible, based on the I_{610}/I_{540} as the signal. The applicability of this probe was confirmed by imaging of endogenous H_2S in HeLa cells and zebrafish.

Wong et al developed **52** with both an aza-18-crown for binding of either Cu^{2+} or Na^+ and a pyridine antenna (Fig. 30). This allows a switch whereby binding of the Cu^{2+} ion results in 17-fold quenching of the luminescence [169]. Further addition of H_2S does not only restore the original emission due to CuS precipitation but induces a further 40-fold increase of luminescence, due to the subsequent binding of Na_2S. The detection limit is about 60 nM. A derivative was prepared wherein the copper binding site was replaced by bis[(2-picolyl)amine] (**53**, Fig. 30) [170]. This complex showed an efficient 8-fold difference in luminescence between the quenched and unquenched complex. There were no observable responses from a variety of different biological molecules especially GSH and cysteine, the complex remained selective for the H_2S added in the form Na_2S. The reported detection limit was 9.6×10^{-4} μM.

A more recent example by Tuck *et al.* [171], demonstrated very efficient 73-fold enhancement of the luminescence in the presence of sulphide, with very fast reaction times and a low detection limit of 130 nM. This complex (**54**, Fig. 30) is built from a DO3A macrocycle functionalized by a pyridine-triazole-bis[(2-picolyl)amine] unit. It operates according to the same mechanism as above for H_2S detection, with the bis[(2-picolyl)amine] moiety acting as copper chelating site.

A ligand showing two distinct cyclen units was designed by Miller et al (**55**, **56**) [172]. One cavity is specific for Eu^{3+} / Tb^{3+} while the other is specific for Cu^{2+}. A quinoline chromophore was incorporated in order to maximise sensitisation of the Ln^{3+}. Sensitised Tb^{3+} luminescence was quenched in the presence of Cu^{II}. Addition of H_2S leads to a >100 fold increase in luminescence based on a demetallation strategy (Fig. 30), with a detection limit greater than 10 nM. This complex is cell permeable and also demonstrates, once incorporated, a response to added Na_2S.

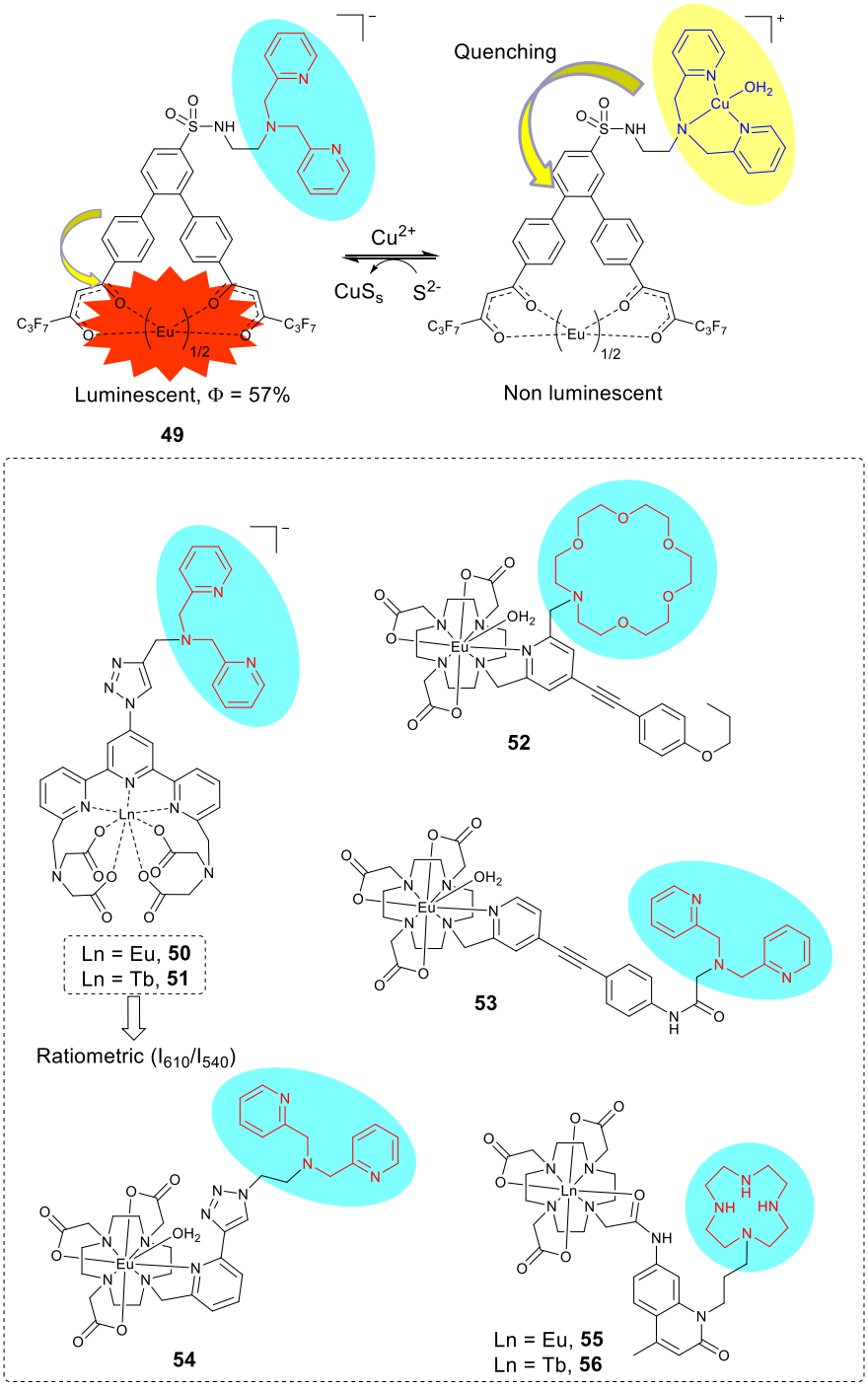

Figure 30. Lanthanide complexes for the switch on detection of H_2S or S^{2-}. The mechanism with cooperative copper binding and release is indicated for complex **49**. The copper chelating site is depicted in red.

9. Other redox-responding lanthanide probes

Some lanthanide probes were designed for responding to the whole redox status (or redox potential) and not a distinct ROS, RNS or sulfur-based compound. We will

comment in this section only those whereby the ligand can act a redox switch under non "extreme" conditions.

9.1 Magnetic resonance imaging of hypoxia

The DO2amide and DO3A macrocyclic platform were appended by diverse groups to achieve detection of reducing environments or hypoxia.

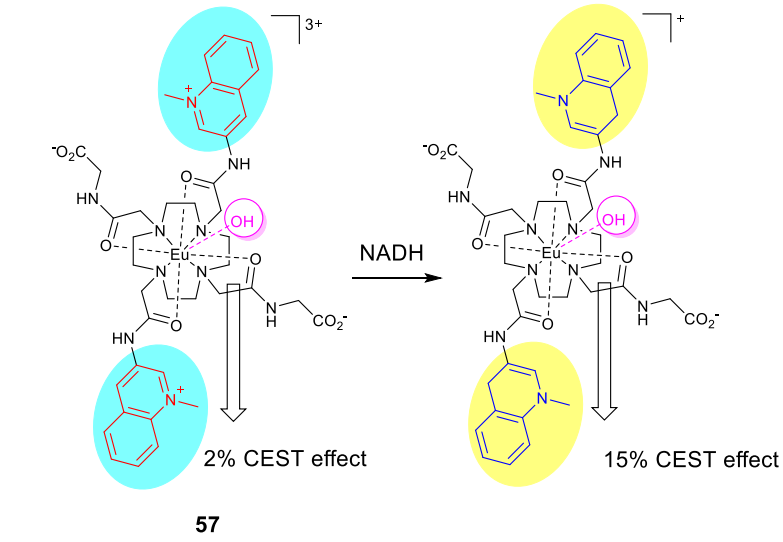

57

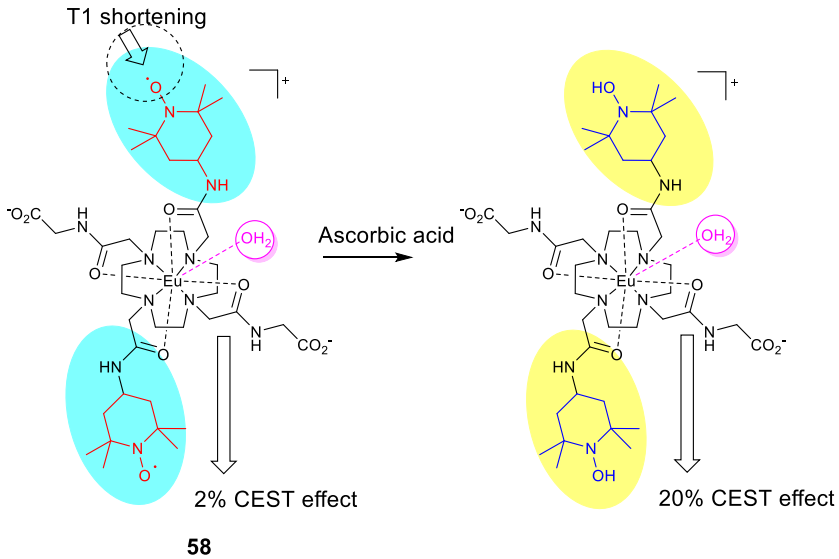

58

Figure 31. Lanthanide complexes featuring a redox-active arm prone to reduction by physiological reductants

The first example exploits the fact that N-methylquinolinium moieties are prone to reduction by NADH into dihydroquinoline in cellular medium [173]. The europium complex **57** (Fig. 31) was nearly CEST-silent, with 2% CEST signal arising from exchange of the Eu^{3+}-bound water molecule. The CEST signal increases significantly (15%) upon reduction with NADH and undergoes a shift from 43 to 50 ppm, with shorter water exchange lifetime. It must be stressed that a nitrophenyl derivative (instead of N-methyquinolinium) was previously shown to undergo a larger change of intensity of CEST signal upon reduction (30%), but the conditions required (40 psi H_2 over Pd/C in EtOH) are not physiological [174]. The europium complex **58** features two pendent TEMPO radical units and was used as PARACEST sensor for reducing conditions (hypoxia) [175]. The radical complex exhibits a weak CEST signal (2%) due to T1 shortening of bulk water protons by the neighbouring radical units. After reaction with ascorbate the nitroxide units are reduced into diamagnetic hydroxylamines, resulting in an increase in T_1 of the bulk water protons. As a consequence, the CEST signal increases significantly, reaching a 20% effect. Interestingly, this compound accumulates in the bladder after injection due to its low molecular weight and hydrophilicity, although no clear CEST signal was detected. Subsequent administration of ascorbic acid results in strong CEST contrast of the bladder content due to the reduction of the nitroxide moiety. It was proposed, but not yet experimentally proven that hypoxia conditions would favour the *in vivo* reduction of the nitroxide units of **58**.

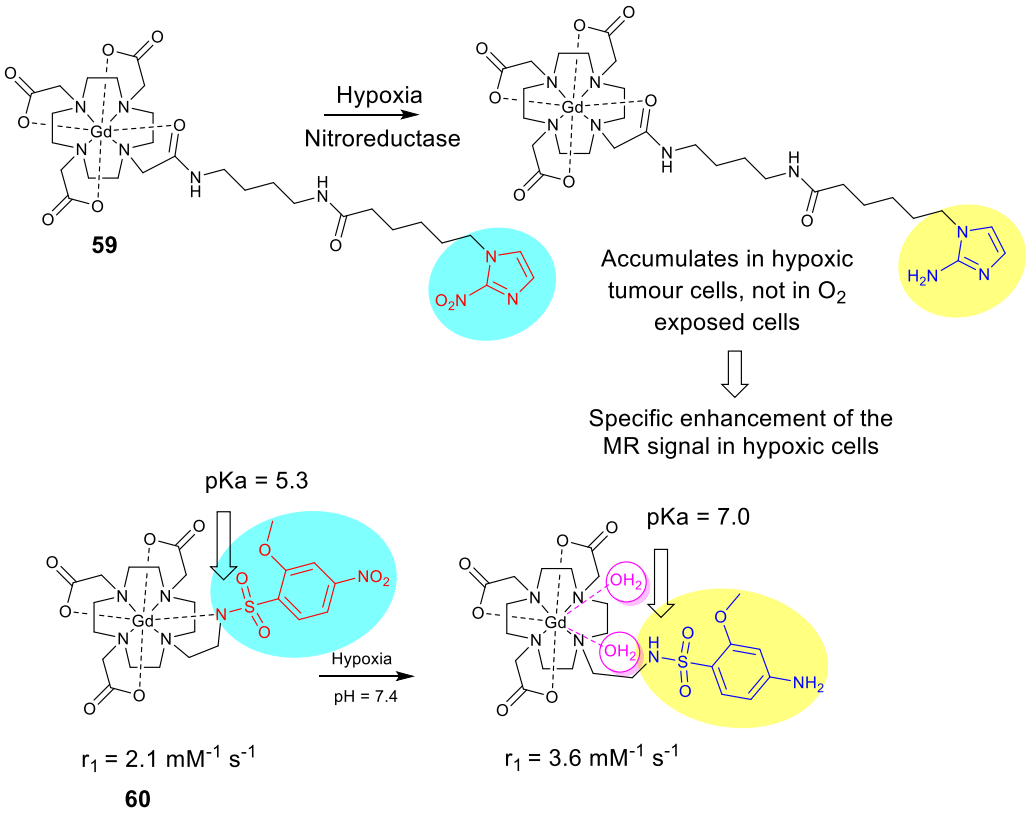

Figure 32. Lanthanide complexes responsive to hypoxia in an irreversible fashion

The hypoxia could be also assessed by exploiting the ability of 2-nitroimidazoles to be selectively reduced by nitroreductases, which are overexpressed under low oxygen conditions. The gadolinium complex **59** (Fig. 32) features both a highly chelating DO3A unit and a long arm ended by a 2-nitroimidazole [176]. *In vitro* studies demonstrate that this neutral complex could enter both hypoxic cells and those maintained under oxygen atmosphere, but **59** is retained only in the first ones. Further *in vivo* studies on prostate tumor xenografts, which are known to be highly hypoxic, confirm that **59** enhances the MR signal in the central region of the tumor. Some nitrophenyl moieties also demonstrated reduction into anilines under hypoxic conditions. The gadolinium complex **60** (Fig. 32) is based on a DO3A unit, similarly to **59**, but was appended by a shorter 2-methoxy-4-nitrobenzenesulfonamide arm [177]. Reduction of the nitro group induces a shift of the pKa of the sulphonamide nitrogen from 5.3 to 7, which triggers the decoordination of this arm at pH close to neutrality. This reaction is associated with the binding of two water molecules, with subsequent change of relaxivity from r_1 = 2.1 mM^{-1} s^{-1} to 3.6 mM^{-1} s^{-1}.

9.2 Luminescence changes associated to electrochemical oxidation

A first example is a propargyl functionalised ligand, which gave the complexes **61-62** (Fig. 33), which is appended by a redox-active ferrocene moiety via click chemistry [178]. Ferrocene displays a ligand to metal charge transfer transition where the extinction coefficient is highly sensitive to the ferrocene redox state. Electrolytic oxidation of the ferrocene moiety (+0.6 V vs Ag^{+}/Ag) induces a reversible quenching of the luminescence by about 25%. For example, the oxidised form of ferrocene sensitises the formation of the Yb $^{2}F_{5/2}$ state but that the low-lying excited states of ferrocenium can act to quench this excited state.

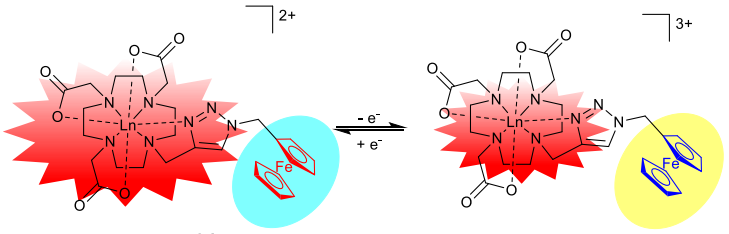

Ln = Yb, **61**
Ln = Eu, **62**

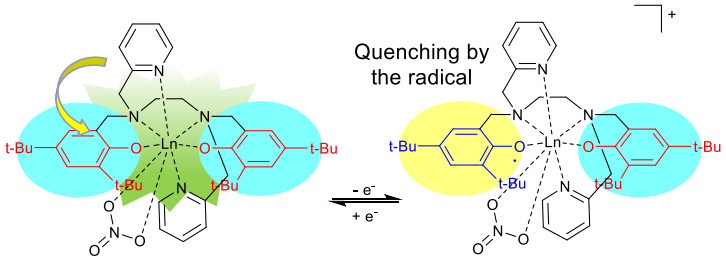

Luminescent
Ln = Yb, **63**
Ln = Tb, **64**

Poorly luminescent

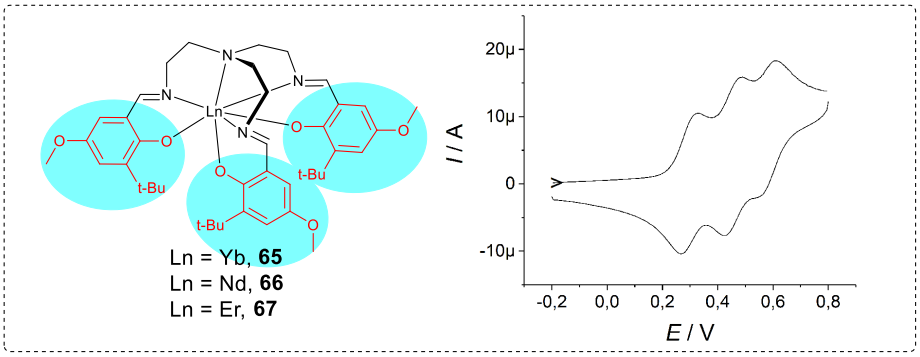

Ln = Yb, **65**
Ln = Nd, **66**
Ln = Er, **67**

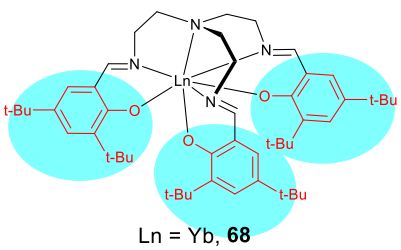

Ln = Yb, **68**
Ln = Tb, **69**

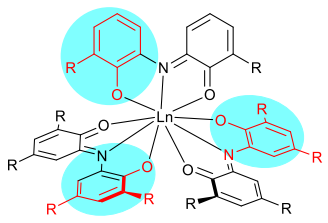

Ln = Yb, **70**
Ln = Eu, **71**

R = t-Bu

Figure 33. Lanthanide complexes appended by a redox-active unit showing a reversibility in the redox process. Insert: cyclic voltammetry curve of **67**, showing the three reversible oxidation waves (ref: Fc^+/Fc).

More recently we prepared the HBED derivatives **63-64** (Fig. 33) [179]. The ligand contains two sensitizing pyridine moieties, as well as two electron-rich di-*tert*-butyl phenolate moieties. These latter were electrochemically oxidized (0.7 vs Fc^+/Fc) into phenoxyl radicals. Phenoxyl radical formation was associated to quenching of the lanthanide (Tb^{3+}, Yb^{3+}) luminescence by up to 95 %. This strategy was also applied to tripodal ligands, wherein three equivalent salicylidene moieties are connected to pivotal nitrogen [180, 181]. Complexes **65-69** are based on both the 2,4-di-*tert*-butylphenol and 2-*tert*-butyl-4-methoxyphenol (Fig. 33). The latter series gives rise to more stable phenoxyl radicals due to the stronger electron-donating ability of the methoxy substituent. Complexes **65-67** are luminescent at room temperature but not their terbium and europium derivatives because of the low energy of the ligand triplet state, with respect to the energy of the Tb($^5D_4$) and Eu($^5D_0$) levels. Again, phenoxyl radical formation results in a quenching of the lanthanide luminescence. The extent of quenching reaches 83, 92 and 79% for **65-67**, respectively. The quenching was in the same range for complex **68** (93%), which features a distinct di-*tert*-butylphenol moiety. The limited hydrophilicity of **65-69** however prevented their use as physiological redox probes. The redox-active aminophenolate moiety was also investigated because of the lower redox potential for radical formation. Complexes **70-71** undergo several ligand-centered redox events, and produce more stable radicals but ligand reabsorption prevents the observation of the metal-centered luminescence, precluding their use as luminescent redox-probes.

10. Advantages of lanthanide complexes over other systems

Real time imaging of these reactive oxygen species, which are very short lived and difficult to detect is essential if a broader understanding of their biological processes is to be understood. The detection of ROS species has been extensively reported previously via organic fluorescent probes, some of them being commercially available (Brite ®, CellROX …), or d-block metal complexes.[87, 116] However simple fluorescent systems have been shown to fall short for specific efficient detection due to short lifetimes and very limited penetration. In particular

sensitivity and detection in tissues where penetration of fluorescent signals is essential is a real problem often displaying broad emission spectra and very short lifetimes in the visible range. In some particular cases the reaction kinetics or the complexity of the required medium can be also a problematic issue. Other methods were developed, based on EPR spectroscopy for radical ROS like $OH^{\bullet}$, as well as electrochemical tools. They proved to be simple and specific, but unfortunately lack sensitivity.[139]

Lanthanide complexes for ROS, RNS and thiols detection as shown above are fascinating as they include very sensitive detection with low detection limits due to longer lifetimes and distinctive emission**.** As an example, the detection of RNS using lanthanide complexes has allowed a significant advantage with respect to classic fluorescent probes, which report limits of detection less efficient than those of sensitive lanthanide probes, lower than 500 nM, whereby ratiometric luminescent detection with Ln^{III} can achieve lower than 5nM detection limits. The concept of using ligands, which can then react with the RNS and then report to the metal ion provoking the response is a relatively novel one to the field. Exceptional detection limits of about 10 nM for the presence of thiols in bimetallic complexes with Cu are other illustrations of the potentiality of lanthanide complexes for detection. Overall, the design of lanthanide complexes thus responds to several criteria which removes the problems of detection limits and tissue penetration with ratiometric probes possible using both luminescent and magnetic responses**.** Additionally, its selective detection is important due to the abundance of other oxygen and nitrogen rich species in biological systems. Lanthanide complexes push the barrier of detection even further, allowing not only specific rapid detection meaning low detection limits but also allowing both luminescent and magnetic techniques to be exploited at the same time. Since the ligand can be specifically altered for activity to ROS species the selectivity can be controlled more easily than in classic organic chromophoric systems. Further developments revolve around two-photons probes, nanoobjects for improved local concentration and of course a faster and selective response, with minimal toxicity.

11. Conclusion

The development of novel molecular materials with new functionality offers promise for their application in innovative imaging techniques. Several decades of intense research demonstrated the potential of lanthanide complexes for biological imaging, especially due to their magnetic and luminescence properties. In particular they offer distinct

advantages as responsive probes for imaging due to their fascinating properties specific to each metal [182]. While unmissable in many fields, they are at first glance unsuitable for redox imaging due to the inherent propensity of most of them to adopt the (+III) oxidation state. Recently a new strategy based on redox-reactive ligands has emerged, which relegates these initial assumptions to the past. The use of such ligands indeed confers on the complexes a redox reactivity or redox response, whereby the ligand acts as a 'detector' and transfers the information to the lanthanide that acts as a reporter. As demonstrated with several interesting examples, the largest advantage of this process is the design and malleability of the ligand system allowing the reactivity or redox activity to be tuned as a function of the design of the ligand. This flexibility is a huge advantage in the design of specific probes, particularly allowing large scale synthesis of effective ligands before complexation and testing. The lanthanide properties then confer very specific detectable signals, which allow more specific detection and lower detection limits. These probes however, being metal based must provide several requirements to be really applicable in biological imaging including high selectivity, effectiveness in biological media and low toxicity.

These promising results pave the way for new smart lanthanide probes, expanding the scope of applications of lanthanide complexes to domains yet under developed.

Conflicts of interest

The authors declare no conflicts of interest.

Acknowledgements

The authors thank French National Research Agency in the framework of the "Investissements d'avenir" program (ANR-15-IDEX-02), Labex ARCANE, CBH-EUR-GS (ANR-17-EURE-0003) and ANR Co-Lantha (ANR-17-CE07-0034).

Notes and references

[1] M.J. Weber, Lanthanide and Actinide Lasers, in: Lanthanide and Actinide Chemistry and Spectroscopy, American Chemical Society, 1980, pp. 275-311. https://doi.org/10.1021/bk-1980-0131.ch014.

[2] D.N. Woodruff, R.E.P. Winpenny, R.A. Layfield, Chem. Rev., 113 (2013) 5110-5148. https://doi.org/10.1021/cr400018q.
[3] S.-B. Xia, F.-S. Li, X. Shen, X. Li, F.-X. Cheng, C.-K. Sun, H. Guo, J.-J. Liu, Mat. Lett., 238 (2019) 171-174. https://www.sciencedirect.com/science/article/pii/S0167577X18319530.
[4] H. Pellissier, Coord. Chem. Rev., 336 (2017) 96-151. https://www.sciencedirect.com/science/article/pii/S0010854516305331.
[5] X. Qin, X. Liu, W. Huang, M. Bettinelli, X. Liu, Chem. Rev., 117 (2017) 4488-4527. https://doi.org/10.1021/acs.chemrev.6b00691.
[6] L.E. MacKenzie, R. Pal, Nature Rev. Chem., 5 (2021) 109-124. https://doi.org/10.1038/s41570-020-00235-4.
[7] R.D. Teo, J. Termini, H.B. Gray, J. Med. Chem., 59 (2016) 6012-6024. https://doi.org/10.1021/acs.jmedchem.5b01975.
[8] G.C. Pimentel, R.D. Sprately, Understanding Chemistry, Holden-Day Inc., San Francisco, CA., 1971.
[9] H.M. Nicholas, D.P. Mills, Lanthanides: Divalent Organometallic Chemistry, in: Encyclopedia of Inorganic and Bioinorganic Chemistry, 2011, pp. 1-10. https://onlinelibrary.wiley.com/doi/abs/10.1002/9781119951438.eibc2453.
[10] C.T. Palumbo, I. Zivkovic, R. Scopelliti, M. Mazzanti, J. Am. Chem. Soc., 141 (2019) 9827-9831. https://doi.org/10.1021/jacs.9b05337.
[11] N.T. Rice, I.A. Popov, D.R. Russo, T.P. Gompa, A. Ramanathan, J. Bacsa, E.R. Batista, P. Yang, H.S. La Pierre, Chem. Sci., 11 (2020) 6149-6159. http://dx.doi.org/10.1039/D0SC01414A.
[12] T.P. Gompa, A. Ramanathan, N.T. Rice, H.S. La Pierre, Dalton Trans., 49 (2020) 15945-15987. http://dx.doi.org/10.1039/D0DT01400A.
[13] C. Tu, A.Y. Louie, Chem. Commun., (2007) 1331-1333. http://dx.doi.org/10.1039/B616991K.
[14] Q.N. Do, J.S. Ratnakar, Z. Kovács, A.D. Sherry, ChemMedChem, 9 (2014) 1116-1129. https://chemistry-europe.onlinelibrary.wiley.com/doi/abs/10.1002/cmdc.201402034.
[15] P.B. Tsitovich, P.J. Burns, A.M. McKay, J.R. Morrow, J. Inorg. Biochem., 133 (2014) 143-154. https://www.sciencedirect.com/science/article/pii/S0162013414000208.
[16] S.M. Pinto, V. Tomé, M.J.F. Calvete, M.M.C.A. Castro, É. Tóth, C.F.G.C. Geraldes, Coord. Chem. Rev., 390 (2019) 1-31. https://www.sciencedirect.com/science/article/pii/S0010854519300591.
[17] L. Wu, A.C. Sedgwick, X. Sun, S.D. Bull, X.-P. He, T.D. James, Acc. Chem .Rev., 52 (2019) 2582-2597. https://doi.org/10.1021/acs.accounts.9b00302.
[18] Q.N. Do, J.S. Ratnakar, Z. Kovács, A.D. Sherry, ChemMedChem, 9 (2014) 1116-1129. http:https://doi.org/10.1002/cmdc.201402034.
[19] P. Bonnitcha, S. Grieve, G. Figtree, Free Rad. Biol. Med., 126 (2018) 296-312. https://www.sciencedirect.com/science/article/pii/S0891584918314011.
[20] R. Zhang, J. Yuan, Acc. Chem .Rev., 53 (2020) 1316-1329. https://doi.org/10.1021/acs.accounts.0c00172.
[21] D. Trachootham, W. Lu, M.A. Ogasawara, N.R.-D. Valle, P. Huang, Antiox. Redox. Sign., 10 (2008) 1343-1374. https://www.liebertpub.com/doi/abs/10.1089/ars.2007.1957.
[22] I. Liguori, G. Russo, F. Curcio, G. Bulli, L. Aran, D. Della-Morte, G. Gargiulo, G. Testa, F. Cacciatore, D. Bonaduce, P. Abete, Clin. interv. aging, 13 (2018) 757-772. https://doi.org/10.2147/CIA.S158513.
[23] B. Marengo, M. Nitti, A.L. Furfaro, R. Colla, C.D. Ciucis, U.M. Marinari, M.A. Pronzato, N. Traverso, C. Domenicotti, Oxid. Med. Cell. Longev., 2016 (2016) 6235641. https://doi.org/10.1155/2016/6235641.
[24] F. Collin, Int. J. Mol. Sci., 20 (2019) 2407. https://www.mdpi.com/1422-0067/20/10/2407.
[25] J.-C.G. Bünzli, S.V. Eliseeva, Chem. Sci., 4 (2013) 1939-1949. http://dx.doi.org/10.1039/C3SC22126A.
[26] S.V. Eliseeva, J.-C.G. Bünzli, Chem. Soc. Rev., 39 (2010) 189-227. http://dx.doi.org/10.1039/B905604C.
[27] K. Binnemans, Chem. Rev., 109 (2009) 4283-4374. https://doi.org/10.1021/cr8003983.
[28] B. D'Autréaux, M.B. Toledano, Nature Rev. Mol. Cell Biol., 8 (2007) 813-824. https://doi.org/10.1038/nrm2256.

[29] J.F. Gielis, P.A.J. Beckers, J.J. Briedé, P. Cos, P.E. Van Schil, Ann. Transl. Med., 5 (2017) 4. http://atm.amegroups.com/article/view/14070.
[30] M. Forkink, J.A.M. Smeitink, R. Brock, P.H.G.M. Willems, W.J.H. Koopman, Biochim. Biophys. Acta, 1797 (2010) 1034-1044. https://www.sciencedirect.com/science/article/pii/S000527281000023X.
[31] G. Ferrer-Sueta, R. Radi, ACS Chemical Biology, 4 (2009) 161-177. https://doi.org/10.1021/cb800279q.
[32] A. Phaniendra, D.B. Jestadi, L. Periyasamy, Ind. J. Clin. Biochem., 30 (2015) 11-26. https://doi.org/10.1007/s12291-014-0446-0.
[33] B.C. Dickinson, C.J. Chang, Nature Chem. Biol., 7 (2011) 504-511. https://doi.org/10.1038/nchembio.607.
[34] J.F. Turrens, Formation of Reactive Oxygen Species in Mitochondria, in: S.M. Schaffer S.W. (Ed.) Mitochondria. Advances in Biochemistry in Health and Disease, Springer, New York, NY., 2007, pp. 185-196. https://doi.org/10.1007/978-0-387-69945-5_8.
[35] H. Dancygier, P. Schirmacher, Free Radicals, Reactive Oxygen Species, Oxidative and Endoplasmic Reticulum Stress., in: Clinical Hepatology, Springer, Berlin, Heidelberg, 2010. https://doi.org/10.1007/978-3-540-93842-2_14.
[36] C. Lismont, M. Nordgren, P.P. Van Veldhoven, M. Fransen, Front .Cell Dev. Biol., 3 (2015) 35-35. https://doi.org/10.3389/fcell.2015.00035.
[37] M.G. Battelli, L. Polito, M. Bortolotti, A. Bolognesi, Oxid. Med. Cell. Longev., (2016) Article ID 3527579. https://doi.org/10.1155/2016/3527579.
[38] E.E. Kelley, N.K.H. Khoo, N.J. Hundley, U.Z. Malik, B.A. Freeman, M.M. Tarpey, Free Rad. Biol. Med., 48 (2010) 493-498. https://www.sciencedirect.com/science/article/pii/S0891584909007254.
[39] A.M. Pisoschi, A. Pop, Eur. J. Med. Chem., 97 (2015) 55-74. https://doi.org/10.1016/j.ejmech.2015.04.040.
[40] K. Samardzic, K.J. Rodgers, Biol. Chem., 398 (2017) 1165-1175. https://doi.org/10.1515/hsz-2017-0124.
[41] J. Cadet, J.R. Wagner, Cold Spring Harb. Perspect. Biol., 5 (2013). http://cshperspectives.cshlp.org/content/5/2/a012559.abstract.
[42] R. Radi, Proc. Nat. Acad. Sci. U.S.A., 115 (2018) 5839-5848. https://www.pnas.org/content/pnas/115/23/5839.full.pdf.
[43] M.E. Stroupe, M. DiDonato, J.A. Tainer, Manganese Superoxide Dismutase, in: Handbook of Metalloproteins, 2004. https://onlinelibrary.wiley.com/doi/abs/10.1002/0470028637.met167.
[44] D. Bordo, A. Pesce, M. Bolognesi, M. Elena Stroppolo, M. Falconi, A. Desideri, Copper-Zinc Superoxide Dismutase in Prokaryotes and Eukaryotes, in: Handbook of Metalloproteins, 2004. https://onlinelibrary.wiley.com/doi/abs/10.1002/0470028637.met194.
[45] M.J. Maté, G. Murshudov, J. Bravo, W. Melik-Adamyan, P.C. Loewen, I. Fita, Heme-Catalases, in: Handbook of Metalloproteins, 2004. https://onlinelibrary.wiley.com/doi/abs/10.1002/0470028637.met134.
[46] M. Gajhede, Horseradish Peroxidase, in: Handbook of Metalloproteins, 2004. https://onlinelibrary.wiley.com/doi/abs/10.1002/0470028637.met116.
[47] J. Nordberg, E.S.J. Arnér, Free Rad. Biol. Med., 31 (2001) 1287-1312. https://www.sciencedirect.com/science/article/pii/S0891584901007249.
[48] A. Meister, J. Biol. Chem., 263 (1988) 17205-17208. http://www.jbc.org/content/263/33/17205.short.
[49] R. Figueroa-Méndez, S. Rivas-Arancibia, Front Physiol, 6 (2015) 397-397. https://doi.org/10.3389/fphys.2015.00397.
[50] Y.K. Nakamura, S.T. Omaye, J. Funct. Food, 1 (2009) 241-252. https://www.sciencedirect.com/science/article/pii/S1756464609000164.
[51] Y.Y. Sautin, R.J. Johnson, Nucleosides Nucleotides Nucleic Acids, 27 (2008) 608-619. https://doi.org/10.1080/15257770802138558.
[52] K.B. Beckman, B.N. Ames, Physiol. Rev., 78 (1998) 547-581. https://doi.org/10.1152/physrev.1998.78.2.547.

[53] M. Brownlee, Nature, 414 (2001) 813-820. https://doi.org/10.1038/414813a.
[54] D. Gradinaru, C. Borsa, C. Ionescu, G.I. Prada, Mech. Ageing Dev., 151 (2015) 101-113. https://www.sciencedirect.com/science/article/pii/S0047637415000287.
[55] E. Verhoye, M.R. Langlois, Clin. Chem. Lab. Med., 47 (2009) 128-137. https://doi.org/10.1515/CCLM.2009.037.
[56] E. Tönnies, E. Trushina, J. Alzheimers Dis., 57 (2017) 1105-1121. https://pubmed.ncbi.nlm.nih.gov/28059794

https://www.ncbi.nlm.nih.gov/pmc/articles/PMC5409043/.
[57] J.E. Klaunig, L.M. Kamendulis, B.A. Hocevar, Toxicol. Pathol., 38 (2010) 96-109. https://doi.org/10.1177/0192623309356453.
[58] K. Ghosh, B.C. Capell, J. Invest. Dermatol., 136 (2016) 2133-2139. http://www.sciencedirect.com/science/article/pii/S0022202X1632098X.
[59] S.G. Jarrett, M.E. Boulton, Mol. Aspects Med., 33 (2012) 399-417. https://www.sciencedirect.com/science/article/pii/S0098299712000386.
[60] S. Abokyi, C.-H. To, T.T. Lam, D.Y. Tse, Oxid. Med. Cell. Longev., 2020 (2020) 7901270. https://doi.org/10.1155/2020/7901270.
[61] O. Adeoye, J. Olawumi, A. Opeyemi, O. Christiania, JBRA Assist. Reprod., 22 (2018) 61-66. https://doi.org/10.5935/1518-0557.20180003.
[62] P. Pacher, J.S. Beckman, L. Liaudet, Physiol. Rev., 87 (2007) 315-424. https://journals.physiology.org/doi/abs/10.1152/physrev.00029.2006.
[63] B.C. Dickinson, C.J. Chang, Nat. Chem. Biol., 7 (2011) 504-511.
[64] G. Ferrer-Sueta, N. Campolo, M. Trujillo, S. Bartesaghi, S. Carballal, N. Romero, B. Alvarez, R. Radi, Chem. Rev., 118 (2018) 1338-1408. https://doi.org/10.1021/acs.chemrev.7b00568.
[65] M.R. Reynolds, R.W. Berry, L.I. Binder, Biochemistry, 44 (2005) 1690-1700. https://doi.org/10.1021/bi047982v.
[66] G.-P. Yan, L. Robinson, P. Hogg, Radiography, 13 (2007) e5-e19. http://www.sciencedirect.com/science/article/pii/S1078817406000885.
[67] M.F. Tweedle, J. Am. Chem. Soc., 124 (2002) 884-885. https://doi.org/10.1021/ja0152963.
[68] K. Chen, X. Chen, Curr. Top. Med. Chem., 10 (2010) 1227-1236. https://www.eurekaselect.com/86009/article.
[69] G. Liang, P.K. Nguyen, J. Nuc. Cardiol., 23 (2016) 783-789. https://doi.org/10.1007/s12350-016-0501-8.
[70] H. Li, T.J. Meade, J. Am. Chem. Soc., 141 (2019) 17025-17041. https://doi.org/10.1021/jacs.9b09149.
[71] L. Helm, J.R. Morrow, C.J. Bond, F. Carniato, M. Botta, M. Braun, Z. Baranyai, R. Pujales-Paradela, M. Regueiro-Figueroa, D. Esteban-Gómez, C. Platas-Iglesias, T.J. Scholl, Chapter 2 Gadolinium-based Contrast Agents, in: Contrast Agents for MRI: Experimental Methods, The Royal Society of Chemistry, 2018, pp. 121-242. http://dx.doi.org/10.1039/9781788010146-00121.
[72] S. Lacerda, É. Tóth, ChemMedChem, 12 (2017) 883-894. https://doi.org/10.1002/cmdc.201700210.
[73] M. Bottrill, L. Kwok, N.J. Long, Chem. Soc. Rev., 35 (2006) 557-571. http://dx.doi.org/10.1039/B516376P.
[74] E.J. Werner, A. Datta, C.J. Jocher, K.N. Raymond, Angew. Chem. Int. Ed., 47 (2008) 8568-8580. https://onlinelibrary.wiley.com/doi/abs/10.1002/anie.200800212.
[75] L.M. De León-Rodríguez, A.F. Martins, M.C. Pinho, N.M. Rofsky, A.D. Sherry, J. Magn. Reson. Imaging, 42 (2015) 545-565. https://onlinelibrary.wiley.com/doi/abs/10.1002/jmri.24787.
[76] M.L. James, S.S. Gambhir, Physiol. Rev., 92 (2012) 897-965. https://journals.physiology.org/doi/abs/10.1152/physrev.00049.2010.
[77] M.C. Heffern, L.M. Matosziuk, T.J. Meade, Chem. Rev., 114 (2014) 4496-4539. https://doi.org/10.1021/cr400477t.

[78] G. Wang, G. Angelovski, Angew. Chem. Int. Ed., 60 (2021) 5734-5738. https://onlinelibrary.wiley.com/doi/abs/10.1002/anie.202014431.
[79] K.M. Ward, A.H. Aletras, R.S. Balaban, J. Magn. Res., 143 (2000) 79-87. https://www.sciencedirect.com/science/article/pii/S1090780799919560.
[80] A.D. Sherry, M. Woods, Ann. Rev. Biomed. Eng., 10 (2008) 391-411. https://www.annualreviews.org/doi/abs/10.1146/annurev.bioeng.9.060906.151929.
[81] S. Zhang, M. Merritt, D.E. Woessner, R.E. Lenkinski, A.D. Sherry, Acc. Chem .Rev., 36 (2003) 783-790. https://doi.org/10.1021/ar020228m.
[82] M. Woods, D.E. Woessner, A.D. Sherry, Chem. Soc. Rev., 35 (2006) 500-511. http://dx.doi.org/10.1039/B509907M.
[83] V.C. Pierre, S.M. Harris, S.L. Pailloux, Acc. Chem .Rev., 51 (2018) 342-351. https://doi.org/10.1021/acs.accounts.7b00301.
[84] I. Hancu, W.T. Dixon, M. Woods, E. Vinogradov, A.D. Sherry, R.E. Lenkinski, Acta Radiologica, 51 (2010) 910-923. https://doi.org/10.3109/02841851.2010.502126.
[85] A.M. Funk, V. Clavijo Jordan, A.D. Sherry, S.J. Ratnakar, Z. Kovacs, Angew. Chem. Int. Ed., 55 (2016) 5024-5027. https://onlinelibrary.wiley.com/doi/abs/10.1002/anie.201511649.
[86] D. Parker, J.D. Fradgley, K.-L. Wong, Chemical Society Reviews, (2021). http://dx.doi.org/10.1039/D1CS00310K.
[87] N. Kwon, D. Kim, K.M.K. Swamy, J. Yoon, Coord. Chem. Rev., 427 (2021) 213581. https://www.sciencedirect.com/science/article/pii/S0010854520305749.
[88] C.S. Creaser, J.R. Sodeau, Luminescence Spectroscopy, in: D.L. Andrews (Ed.) Perspectives in Modern Chemical Spectroscopy, Springer Berlin Heidelberg, Berlin, Heidelberg, 1990, pp. 103-136. https://doi.org/10.1007/978-3-642-75456-2_5.
[89] D. Tu, W. Zheng, Y. Liu, H. Zhu, X. Chen, Coord. Chem. Rev., 273-274 (2014) 13-29. https://www.sciencedirect.com/science/article/pii/S0010854513002658.
[90] G.-Q. Jin, Y. Ning, J.-X. Geng, Z.-F. Jiang, Y. Wang, J.-L. Zhang, Inorg. Chem. Front., 7 (2020) 289-299. http://dx.doi.org/10.1039/C9QI01132C.
[91] A.T. Bui, M. Beyler, Y.-Y. Liao, A. Grichine, A. Duperray, J.-C. Mulatier, B.L. Guennic, C. Andraud, O. Maury, R. Tripier, Inorg. Chem., 55 (2016) 7020-7025. https://doi.org/10.1021/acs.inorgchem.6b00891.
[92] C.S. Lim, B.R. Cho, BMB Rep., 46 (2013) 188-194. https://doi.org/10.5483/BMBRep.2013.46.4.045.
[93] M.H.V. Werts, Near-Infrared Luminescent Labels and Probes Based on Lanthanide Ions and Their Potential for Applications in Bioanalytical Detection and Imaging, in: P. Hänninen, H. Härmä (Eds.) Lanthanide Luminescence: Photophysical, Analytical and Biological Aspects, Springer Berlin Heidelberg, Berlin, Heidelberg, 2011, pp. 133-159. https://doi.org/10.1007/4243_2010_9.
[94] J.-C.G. Bünzli, S.V. Eliseeva, Basics of Lanthanide Photophysics, in: P. Hänninen, H. Härmä (Eds.) Lanthanide Luminescence: Photophysical, Analytical and Biological Aspects, Springer Berlin Heidelberg, Berlin, Heidelberg, 2011, pp. 1-45. https://doi.org/10.1007/4243_2010_3.
[95] J.-C.G. Bünzli, C. Piguet, Chem. Soc. Rev., 34 (2005) 1048-1077. http://dx.doi.org/10.1039/B406082M.
[96] S.E. Bodman, S.J. Butler, Chem. Sci., 12 (2021) 2716-2734. http://dx.doi.org/10.1039/D0SC05419D.
[97] G. Mathis, H. Bazin, Stable Luminescent Chelates and Macrocyclic Compounds, in: P. Hänninen, H. Härmä (Eds.) Lanthanide Luminescence: Photophysical, Analytical and Biological Aspects, Springer Berlin Heidelberg, Berlin, Heidelberg, 2011, pp. 47-88. https://doi.org/10.1007/4243_2010_5.
[98] A.J. Amoroso, S.J.A. Pope, Chem. Soc. Rev., 44 (2015) 4723-4742. http://dx.doi.org/10.1039/C4CS00293H.
[99] L. Norel, O. Galangau, H. Al Sabea, S. Rigaut, ChemPhotoChem, n/a (2020). https://chemistry-europe.onlinelibrary.wiley.com/doi/abs/10.1002/cptc.202000248.
[100] M.A. Hay, C. Boskovic, Chem. Eur. J., 27 (2021) 3608-3637. https://chemistry-europe.onlinelibrary.wiley.com/doi/abs/10.1002/chem.202003761.

[101] D.W. Siemann, M.R. Horsman, Pharmacol. Ther., 153 (2015) 107-124. http://www.sciencedirect.com/science/article/pii/S0163725815001217.
[102] G.-L. Law, R. Pal, L.O. Palsson, D. Parker, K.-L. Wong, Chem. Commun., (2009) 7321-7323. http://dx.doi.org/10.1039/B920222F.
[103] T. Gunnlaugsson, D. Parker, J. Williams, in: Proc. SPIE, 1999, pp. 3602.
[104] R. Hueting, M. Tropiano, S. Faulkner, RSC Advances, 4 (2014) 44162-44165. http://dx.doi.org/10.1039/C4RA09271F.
[105] H. Nakai, T. Goto, K. Kitagawa, K. Nonaka, T. Matsumoto, S. Ogo, Chem. Commun., 50 (2014) 15737-15739. http://dx.doi.org/10.1039/C4CC07717B.
[106] H. Nakai, K. Nonaka, T. Goto, J. Seo, T. Matsumoto, S. Ogo, Dalton Trans., 44 (2015) 10923-10927. http://dx.doi.org/10.1039/C5DT00816F.
[107] A. Watkis, R. Hueting, T.J. Sørensen, M. Tropiano, S. Faulkner, Chem. Commun., 51 (2015) 15633-15636. http://dx.doi.org/10.1039/C5CC06891F.
[108] H. Zhao, L. Zang, L. Wang, F. Qin, Z. Zhang, W. Cao, Sens. Actuators B Chem., 215 (2015) 405-411. https://www.sciencedirect.com/science/article/pii/S0925400515004153.
[109] H. Nakai, J. Seo, K. Kitagawa, T. Goto, T. Matsumoto, S. Ogo, Dalton Trans., 45 (2016) 9492-9496. http://dx.doi.org/10.1039/C6DT01057A.
[110] H. Nakai, J. Seo, K. Kitagawa, T. Goto, K. Nonaka, T. Matsumoto, S. Ogo, Inorg. Chem., 55 (2016) 6609-6615. https://doi.org/10.1021/acs.inorgchem.6b00800.
[111] T.J. Sørensen, A.M. Kenwright, S. Faulkner, Chem. Sci., 6 (2015) 2054-2059. http://dx.doi.org/10.1039/C4SC03827D.
[112] E. Di Gregorio, G. Ferrauto, E. Gianolio, S. Lanzardo, C. Carrera, F. Fedeli, S. Aime, ACS Nano, 9 (2015) 8239-8248. https://doi.org/10.1021/acsnano.5b02604.
[113] L. Burai, R. Scopelliti, É. Tóth, Chem. Commun., (2002) 2366-2367. http://dx.doi.org/10.1039/B206709A.
[114] L.A. Ekanger, M.M. Ali, M.J. Allen, Chem. Commun., 50 (2014) 14835-14838. http://dx.doi.org/10.1039/C4CC07027E.
[115] L.A. Basal, M.D. Bailey, J. Romero, Meser M. Ali, L. Kurenbekova, J. Yustein, R.G. Pautler, M.J. Allen, Chem. Sci., 8 (2017) 8345-8350. http://dx.doi.org/10.1039/C7SC03142D.
[116] H. Gunduz, S. Kolemen, E.U. Akkaya, Coord. Chem. Rev., 429 (2021) 213641. https://www.sciencedirect.com/science/article/pii/S0010854520308729.
[117] M. Tan, B. Song, G. Wang, J. Yuan, Free Rad. Biol. Med., 40 (2006) 1644-1653. https://www.sciencedirect.com/science/article/pii/S0891584906000025.
[118] W.-S. Lo, H. Li, G.-L. Law, W.-T. Wong, K.-L. Wong, J. Lumin., 169 (2016) 549-552. https://www.sciencedirect.com/science/article/pii/S0022231314007650.
[119] J. Sun, B. Song, Z. Ye, J. Yuan, Inorg. Chem., 54 (2015) 11660-11668. https://doi.org/10.1021/acs.inorgchem.5b02458.
[120] T.-H. Dinh, H.-H. Nguyen, M.-H. Nguyen, Inorg. Chem. Commun., 112 (2020) 107727. https://www.sciencedirect.com/science/article/pii/S1387700319311256.
[121] Z. Dai, L. Tian, Y. Xiao, Z. Ye, R. Zhang, J. Yuan, J. Mat. Chem. B, 1 (2013) 924-927. http://dx.doi.org/10.1039/C2TB00350C.
[122] B. Song, G. Wang, M. Tan, J. Yuan, J. Am. Chem. Soc., 128 (2006) 13442-13450. https://doi.org/10.1021/ja062990f.
[123] B. Song, G. Wang, J. Yuan, Chem. Commun., (2005) 3553-3555. http://dx.doi.org/10.1039/B503980K.
[124] B. Song, G. Wang, M. Tan, J. Yuan, New. J. Chem., 29 (2005) 1431-1438. http://dx.doi.org/10.1039/B510611G.
[125] S.N.A. Jenie, S.M. Hickey, Z. Du, D. Sebben, D.A. Brooks, N.H. Voelcker, S.E. Plush, Inorg. Chim. Acta, 462 (2017) 236-240. https://www.sciencedirect.com/science/article/pii/S0020169317301743.
[126] B. Song, Y. Wu, M. Yu, P. Zhao, C. Zhou, G.E. Kiefer, A.D. Sherry, Dalton Trans., 42 (2013) 8066-8069. http://dx.doi.org/10.1039/C3DT50194A.

[127] A.R. Lippert, T. Gschneidtner, C.J. Chang, Chem. Commun., 46 (2010) 7510-7512. http://dx.doi.org/10.1039/C0CC01560A.
[128] E. Pershagen, K.E. Borbas, Angew. Chem. Int. Ed., 54 (2015) 1787-1790. https://onlinelibrary.wiley.com/doi/abs/10.1002/anie.201408560.
[129] E. Pershagen, J. Nordholm, K.E. Borbas, J. Am. Chem. Soc., 134 (2012) 9832-9835. https://doi.org/10.1021/ja3004045.
[130] Z. Ye, J. Chen, G. Wang, J. Yuan, Anal. Chem., 83 (2011) 4163-4169. https://doi.org/10.1021/ac200438g.
[131] M. Liu, Z. Ye, G. Wang, J. Yuan, Talanta, 91 (2012) 116-121. http://www.sciencedirect.com/science/article/pii/S0039914012000343.
[132] K. Zscharnack, T. Kreisig, A.A. Prasse, T. Zuchner, Anal. Chim. Acta, 834 (2014) 51-57. https://www.sciencedirect.com/science/article/pii/S0003267014006126.
[133] M. Harris, J.L. Kolanowski, E.S. O'Neill, C. Henoumont, S. Laurent, T.N. Parac-Vogt, E.J. New, Chem. Commun., 54 (2018) 12986-12989. http://dx.doi.org/10.1039/C8CC07092J.
[134] X. Liu, L. Guo, B. Song, Z. Tang, J. Yuan, Methods Appl. Fluoresc., 5 (2017).
[135] X. Liu, Z. Tang, B. Song, H. Ma, J. Yuan, J. Mat. Chem. B, 5 (2017) 2849-2855. http://dx.doi.org/10.1039/C6TB02991D.
[136] Y. Xiao, R. Zhang, Z. Ye, Z. Dai, H. An, J. Yuan, Anal. Chem., 84 (2012) 10785-10792. https://doi.org/10.1021/ac3028189.
[137] L. Tian, H. Ma, B. Song, Z. Dai, X. Zheng, R. Zhang, K. Chen, J. Yuan, Talanta, 212 (2020) 120760. http://www.sciencedirect.com/science/article/pii/S0039914020300515.
[138] E. Del Giorgio, T.J. Sørensen, Molecules, 25 (2020) 1959. https://www.mdpi.com/1420-3049/25/8/1959.
[139] J.-T. Hou, M. Zhang, Y. Liu, X. Ma, R. Duan, X. Cao, F. Yuan, Y.-X. Liao, S. Wang, W. Xiu Ren, Coordination Chemistry Reviews, 421 (2020) 213457. https://www.sciencedirect.com/science/article/pii/S0010854520303350.
[140] K.L. Peterson, M.J. Margherio, P. Doan, K.T. Wilke, V.C. Pierre, Inorg. Chem., 52 (2013) 9390-9398. https://doi.org/10.1021/ic4009569.
[141] S.E. Page, K.T. Wilke, V.C. Pierre, Chem. Commun., 46 (2010) 2423-2425. http://dx.doi.org/10.1039/B923912J.
[142] J. Hong, Y. Zhuang, X. Ji, X. Guo, Analyst, 136 (2011) 2464-2470. http://dx.doi.org/10.1039/C0AN00914H.
[143] R. Barré, D. Mouchel dit Leguerrier, L. Fedele, D. Imbert, J.K. Molloy, F. Thomas, Chem. Commun., 56 (2020) 435-438. http://dx.doi.org/10.1039/C9CC06524E.
[144] C. Szíjjártó, E. Pershagen, N.O. Ilchenko, K.E. Borbas, Chem. Eur. J., 19 (2013) 3099-3109. https://chemistry-europe.onlinelibrary.wiley.com/doi/abs/10.1002/chem.201203957.
[145] G. Cui, Z. Ye, J. Chen, G. Wang, J. Yuan, Talanta, 84 (2011) 971-976. https://www.sciencedirect.com/science/article/pii/S0039914011002049.
[146] Y. Xiao, Z. Ye, G. Wang, J. Yuan, Inorg. Chem., 51 (2012) 2940-2946. https://doi.org/10.1021/ic202195a.
[147] Y. Chen, W. Guo, Z. Ye, G. Wang, J. Yuan, Chem. Commun., 47 (2011) 6266-6268. http://dx.doi.org/10.1039/C0CC05658H.
[148] L. Tian, Z. Dai, X. Liu, B. Song, Z. Ye, J. Yuan, Anal. Chem., 87 (2015) 10878-10885. https://doi.org/10.1021/acs.analchem.5b02347.
[149] G. Liu, Y. Li, M.D. Pagel, Magn. Reson. Med., 58 (2007) 1249-1256. https://onlinelibrary.wiley.com/doi/abs/10.1002/mrm.21428.
[150] C. Song, Z. Ye, G. Wang, J. Yuan, Y. Guan, Chem. Eur. J., 16 (2010) 6464-6472. https://chemistry-europe.onlinelibrary.wiley.com/doi/abs/10.1002/chem.201000528.
[151] J. Wu, Y. Yang, L. Zhang, H. Wang, M. Yang, J. Yuan, J. Mat. Chem. B, 5 (2017) 2322-2329. http://dx.doi.org/10.1039/C7TB00345E.
[152] J. Wu, H. Liu, Y. Yang, H. Wang, M. Yang, Opt. Mat., 77 (2018) 170-177. https://www.sciencedirect.com/science/article/pii/S0925346718300326.

[153] Y. Wang, B. Li, X. Song, R. Shen, D. Wang, Y. Yang, Y. Feng, C. Cao, G. Zhang, W. Liu, Anal. Chem., 91 (2019) 12422-12427. https://doi.org/10.1021/acs.analchem.9b03024.
[154] C. Breen, R. Pal, M.R.J. Elsegood, S.J. Teat, F. Iza, K. Wende, B.R. Buckley, S.J. Butler, Chem. Sci., 11 (2020) 3164-3170. http://dx.doi.org/10.1039/C9SC06053G.
[155] H.J. Forman, H. Zhang, A. Rinna, Mol. Aspects Med., 30 (2009) 1-12. http://www.sciencedirect.com/science/article/pii/S0098299708000617.
[156] J. Skalska, S. Bernstein, P. Brookes, Chapter Nine - Measurement of Extracellular (Exofacial) Versus Intracellular Protein Thiols, in: E. Cadenas, L. Packer (Eds.) Methods in Enzymology, Academic Press, 2010, pp. 149-164. https://www.sciencedirect.com/science/article/pii/S007668791074009X.
[157] Q. Li, B. Sun, X. Wang, Z. Jin, Y. Zhou, L. Dong, L.-H. Jiang, W. Rong, Antiox. Redox. Sign., 12 (2010) 1179-1189. https://www.liebertpub.com/doi/abs/10.1089/ars.2009.2926.
[158] N.R. Prabhakar, J. Physiol., 591 (2013) 2245-2257. https://physoc.onlinelibrary.wiley.com/doi/abs/10.1113/jphysiol.2012.247759.
[159] B. Jagadish, G.P. Guntle, D. Zhao, V. Gokhale, T.J. Ozumerzifon, A.M. Ahad, E.A. Mash, N. Raghunand, J. Med. Chem., 55 (2012) 10378-10386. https://doi.org/10.1021/jm300736f.
[160] G.P. Guntle, B. Jagadish, E.A. Mash, G. Powis, R.T. Dorr, N. Raghunand, Transl. Oncol., 5 (2012) 190-199. https://www.sciencedirect.com/science/article/pii/S1936523312800076.
[161] G. Digilio, V. Catanzaro, F. Fedeli, E. Gianolio, V. Menchise, R. Napolitano, C. Gringeri, S. Aime, Chem. Commun., (2009) 893-895. http://dx.doi.org/10.1039/B820593K.
[162] V. Menchise, G. Digilio, E. Gianolio, E. Cittadino, V. Catanzaro, C. Carrera, S. Aime, Mol. Pharm., 8 (2011) 1750-1756. https://doi.org/10.1021/mp2001044.
[163] J. Martinelli, M. Fekete, L. Tei, M. Botta, Chem. Commun., 47 (2011) 3144-3146. http://dx.doi.org/10.1039/C0CC05428C.
[164] M. Tropiano, S. Faulkner, Chem. Commun., 50 (2014) 4696-4698. http://dx.doi.org/10.1039/C4CC01095G.
[165] M.K. Thorson, P. Ung, F.M. Leaver, T.S. Corbin, K.L. Tuck, B. Graham, A.M. Barrios, Anal. Chim. Acta, 896 (2015) 160-165. https://www.sciencedirect.com/science/article/pii/S0003267015011630.
[166] Z. Dai, L. Tian, B. Song, Z. Ye, X. Liu, J. Yuan, Anal. Chem., 86 (2014) 11883-11889. https://doi.org/10.1021/ac503611f.
[167] Y. Wang, H. Wang, X. Zhao, Y. Jin, H. Xiong, J. Yuan, J. Wu, New. J. Chem., 41 (2017) 5981-5987. http://dx.doi.org/10.1039/C7NJ00802C.
[168] Z. Tang, B. Song, H. Ma, Y. Shi, J. Yuan, Anal. Chim. Acta, 1049 (2019) 152-160. https://www.sciencedirect.com/science/article/pii/S0003267018312789.
[169] Z. Liang, T.-H. Tsoi, C.-F. Chan, L. Dai, Y. Wu, G. Du, L. Zhu, C.-S. Lee, W.-T. Wong, G.-L. Law, K.-L. Wong, Chem. Sci., 7 (2016) 2151-2156. http://dx.doi.org/10.1039/C5SC04091D.
[170] Y.-W. Yip, G.-L. Law, W.-T. Wong, Dalton Trans., 45 (2016) 928-935. http://dx.doi.org/10.1039/C5DT03627E.
[171] M.L. Aulsebrook, S. Biswas, F.M. Leaver, M.R. Grace, B. Graham, A.M. Barrios, K.L. Tuck, Chem. Commun., 53 (2017) 4911-4914. http://dx.doi.org/10.1039/C7CC01764B.
[172] Y. Yao, L. Delgado-Rivera, H. Samareh Afsari, L. Yin, G.R.J. Thatcher, T.W. Moore, L.W. Miller, Inorg. Chem., 57 (2018) 681-688. https://doi.org/10.1021/acs.inorgchem.7b02533.
[173] S.J. Ratnakar, S. Viswanathan, Z. Kovacs, A.K. Jindal, K.N. Green, A.D. Sherry, J. Am. Chem. Soc., 134 (2012) 5798-5800. https://doi.org/10.1021/ja211601k.
[174] S.J. Ratnakar, M. Woods, A.J.M. Lubag, Z. Kovács, A.D. Sherry, J. Am. Chem. Soc., 130 (2008) 6-7. https://doi.org/10.1021/ja076325y.
[175] S.J. Ratnakar, T.C. Soesbe, L.L. Lumata, Q.N. Do, S. Viswanathan, C.-Y. Lin, A.D. Sherry, Z. Kovacs, J. Am. Chem. Soc., 135 (2013) 14904-14907. https://doi.org/10.1021/ja406738y.
[176] F.A. Rojas-Quijano, G. Tircsó, E. Tircsóné Benyó, Z. Baranyai, H. Tran Hoang, F.K. Kálmán, P.K. Gulaka, V.D. Kodibagkar, S. Aime, Z. Kovács, A.D. Sherry, Chem. Eur. J., 18 (2012) 9669-9676. https://chemistry-europe.onlinelibrary.wiley.com/doi/abs/10.1002/chem.201200266.
[177] S. Iwaki, K. Hanaoka, W. Piao, T. Komatsu, T. Ueno, T. Terai, T. Nagano, Bioorg. Med. Chem. Lett., 22 (2012) 2798-2802. https://www.sciencedirect.com/science/article/pii/S0960894X12002727.

[178] M. Tropiano, N.L. Kilah, M. Morten, H. Rahman, J.J. Davis, P.D. Beer, S. Faulkner, J. Am. Chem. Soc., 133 (2011) 11847-11849. https://pubs.acs.org/doi/abs/10.1021/ja203069s.
[179] J.K. Molloy, O. Jarjayes, C. Philouze, L. Fedele, D. Imbert, F. Thomas, Chem. Commun., 53 (2017) 605-608. http://dx.doi.org/10.1039/C6CC07942C.
[180] J.K. Molloy, C. Philouze, L. Fedele, D. Imbert, O. Jarjayes, F. Thomas, Dalton Trans., 47 (2018) 10742-10751. http://dx.doi.org/10.1039/C8DT01165F.
[181] J.K. Molloy, L. Fedele, O. Jarjayes, C. Philouze, D. Imbert, F. Thomas, Inorg. Chim. Acta, 483 (2018) 609-617. https://www.sciencedirect.com/science/article/pii/S0020169318311848.
[182] A. Thibon, V.C. Pierre, Anal. Bioanal. Chem., 394 (2009) 107-120. https://doi.org/10.1007/s00216-009-2683-2.